SUPPLEMENTAL MATERIAL

Emergence of tissue polarization from synergy of intracellular and extracellular auxin signaling

Krzysztof Wabnik[1,2,3,8] Jürgen Kleine-Vehn[1,2,8,*], Jozef Balla[4], Michael Sauer[1,2,6], Satoshi Naramoto[1,2], Vilém Reinöhl[4], Roeland M.H. Merks[1,2,7], Willy Govaerts[3] and Jiří Friml[1,2,5,*]

[1] Department of Plant Systems Biology, VIB, 9052 Gent, Belgium, [2] Department of Plant Biotechnology and Genetics, Ghent University, 9052 Gent, Belgium, [3] Department of Applied Mathematics and Computer Science, Ghent University, 9000 Gent, Belgium, [4] Department of Plant Biology, Mendel University, 613 00 Brno, Czech Republic, [5] Department of Experimental Biology, Masaryk University, 601 77 Brno, Czech Republic

[6] Present address: Departamento de Genética Molecular de Plantas, Centro Nacional de Biotecnología, Consejo Superior de Investigaciones Científicas, 28049 Madrid, Spain.

[7] Present address: The Netherlands Centrum Wiskunde & Informatica, 1098 XG Amsterdam, The Netherlands.

[8] These authors contributed equally to this work.

[*] Corresponding authors. Department of Plant Systems Biology, VIB, Ghent University, Technologiepark 927, B-9052 Gent, Belgium. Tel.: +32 9 3313800; Fax: +32 9 3313809; E-mail: jiri.friml@psb.vib-ugent.be and jurgen.kleine-vehn@psb.vib-ugent.be

TABLE OF CONTENTS

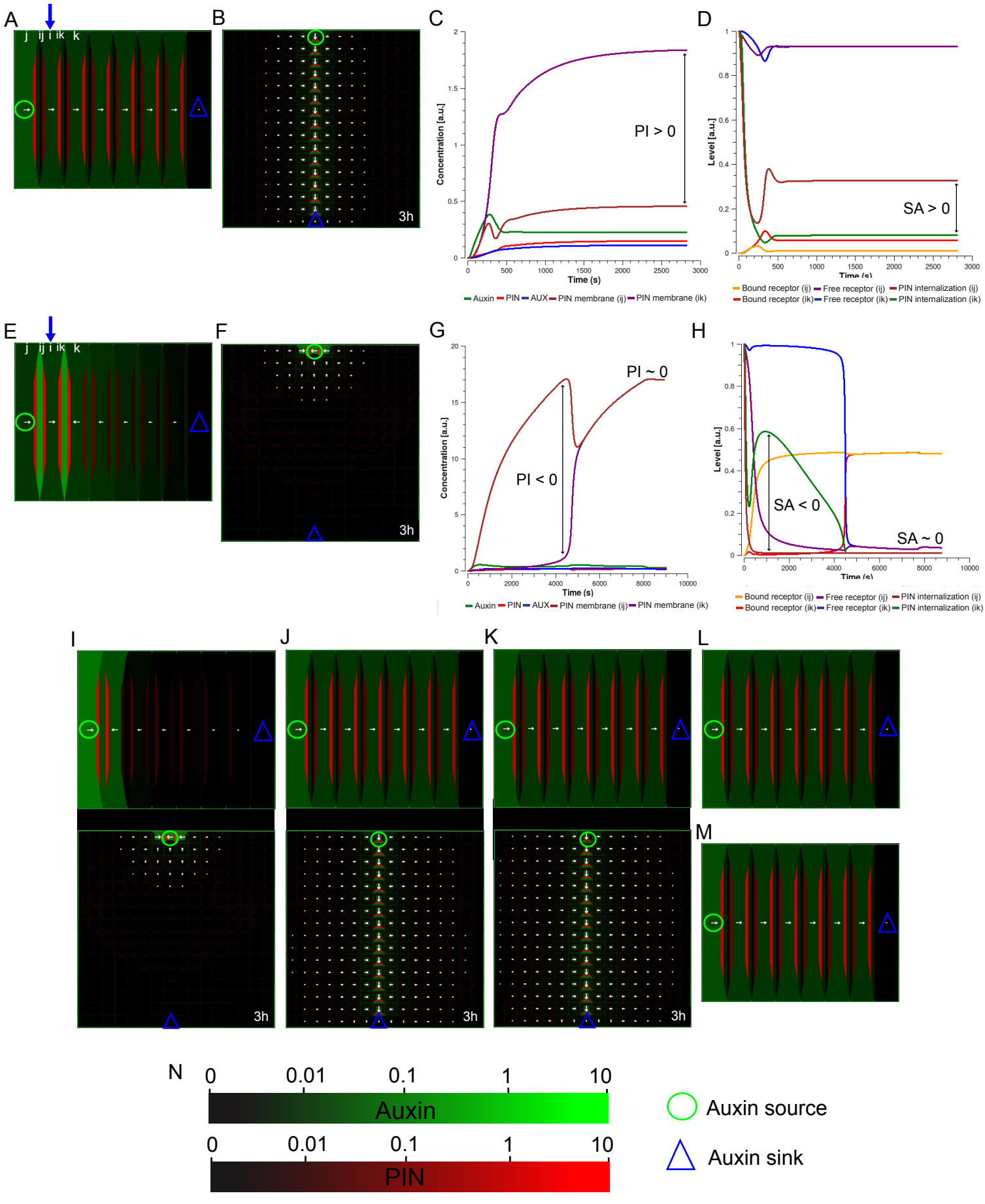
A
j ij i ik k
B
3h
C
PI > 0
Concentration [a.u.]
Time (s)
Auxin PIN AUX PIN membrane (ij) PIN membrane (ik)
D
SA > 0
Level [a.u.]
Time (s)
Bound receptor (ij) Free receptor (ij) PIN internalization (ij)
Bound receptor (ik) Free receptor (ik) PIN internalization (ik)
E
j ij i ik k
F
3h
G
PI ~ 0
PI < 0
Concentration [a.u.]
Time (s)
Auxin PIN AUX PIN membrane (ij) PIN membrane (ik)
H
SA < 0
SA ~ 0
Level [a.u.]
Time (s)
Bound receptor (ij) Free receptor (ij) PIN internalization (ij)
Bound receptor (ik) Free receptor (ik) PIN internalization (ik)
I
J
K
L
M
3h
3h
3h
N
0 0.01 0.1 1 10
Auxin
0 0.01 0.1 1 10
PIN
Auxin source
Auxin sink

Supplementary Figure 1. Model sensitivity with respect to diffusion rates of free and bound auxin receptor.

(A-D) *In silico* 'WT' control simulation **-** Model simulations on the file of cells (A) and on the cellular grid (B) showed PIN polarization and canalization of auxin flow from an auxin source towards a distal auxin sink. Diffusion rate of free receptor (D_R) was set at 1 $\mu m^2 s^{-1}$ and diffusion of bound auxin receptor (D_C) was assumed negligible (~0). **(C)** Time-course profiles of auxin concentration, intracellular PIN and AUX/LAX levels (PIN_i and AUX_i), and PIN membrane levels (PIN_{ij} and PIN_{ik}). **(D)** Time-course profiles of bound (C_{ij} and C_{ik}) and free receptor (R_{ij} and R_{ik}) levels normalized by total amount of receptors in the pool (R_T); and corresponding PIN internalization rates (kh_{ij} and kh_{ik}). Polarization Index (PI) and Signaling Asymmetry (SA) are given to evalutate asymmetry (see also Figure legend 2 for description). **(E-H)** Model simulations on the file of cells (E) and on the cellular grid (F) are presented for diffusion rates of bound and unbound receptor that were equivalent (D_R=D_C=1 $\mu m^2 s^{-1}$). In this case, neither PIN polarization towards an auxin sink nor canalization of auxin flow were observed. This model simulation predicted that neighboring cells tend to pump auxin out to the common cell wall (E, F). Initially, PI and SA were negative, suggesting that more PINs and higher auxin signaling was present at *ij*-th side of the cell. In time they both approach zero which is reflected in non-polar cell behavior (G, H). **(I)** Model simulations on the file of cells and on the cellular grid are presented and diffusion rates of bound and unbound receptor were D_R=1 $\mu m^2 s^{-1}$, D_C=0.1 $\mu m^2 s^{-1}$, **(J)** D_R=1 $\mu m^2 s^{-1}$, D_C=0.001 $\mu m^2 s^{-1}$,**(K)** D_R=0.1 $\mu m^2 s^{-1}$, D_C=0 $\mu m^2 s^{-1}$, **(L)** D_R=10 $\mu m^2 s^{-1}$, D_C=0 $\mu m^2 s^{-1}$, **(M)** D_R=100 $\mu m^2 s^{-1}$, D_C=0 $\mu m^2 s^{-1}$.

A ratio of bound/unbound receptor mobility, denoted as $\alpha = D_C/D_R$ (equations 19-22) directly reflects the asymmetry of signaling on PIN internalization (SA). The lower this ratio is the higher SA becomes. Here, we demonstrated that our model predicts PIN polarization patterns if the diffusion rate of recruited receptors (D_C) is assumed to be at least an order of magnitude lower than the diffusion rate of free soluble receptors (D_R). **(N)** Color coding and symbols are as in Figure 2E and apply to all model simulations.

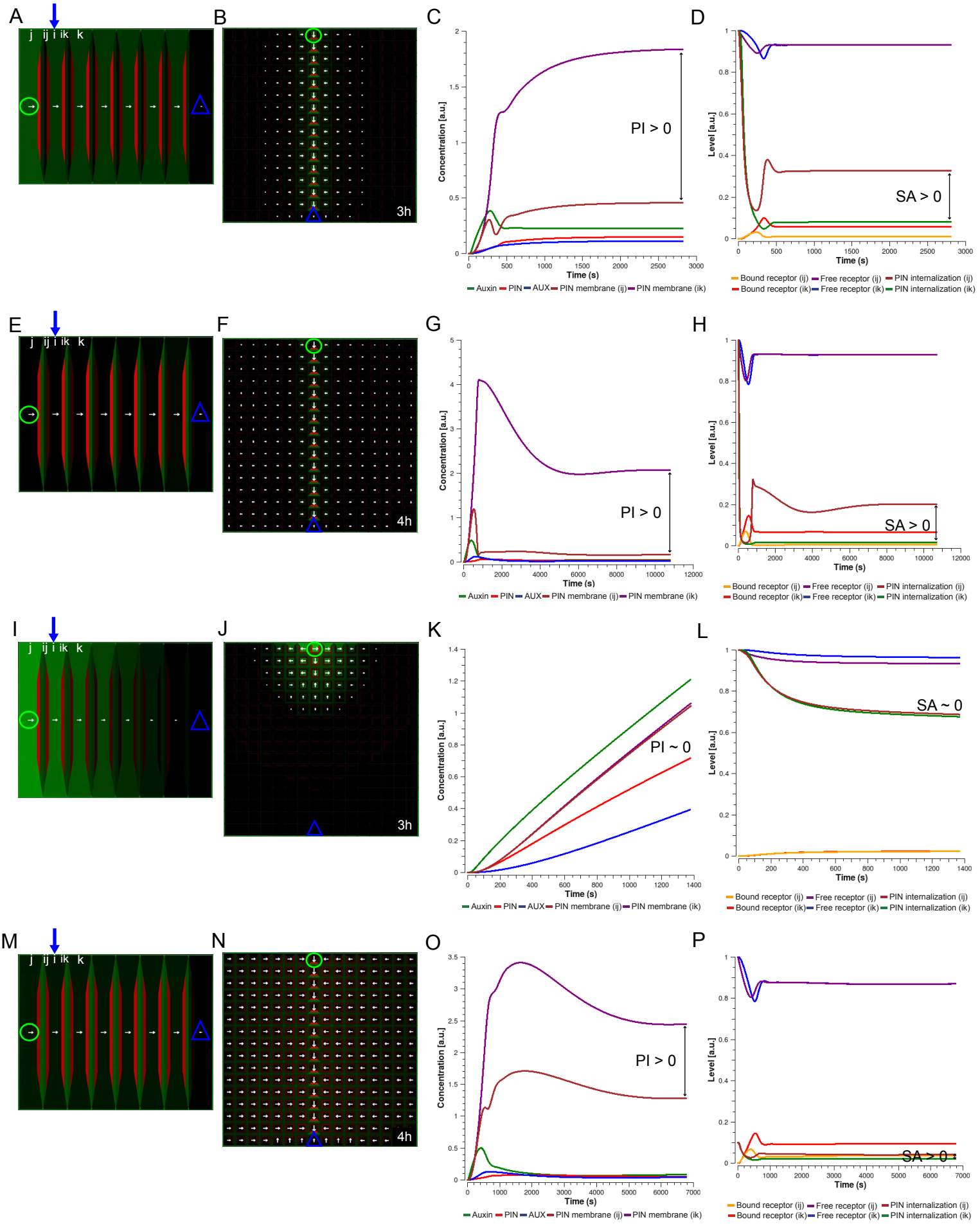
A
B
C
D
E
F
G
H
I
J
K
L
M
N
O
P
j ij i ik k
3h
4h
PI > 0
PI ~ 0
SA > 0
SA ~ 0
Concentration [a.u.]
Level [a.u.]
Time (s)
Auxin
PIN
AUX
PIN membrane (ij)
PIN membrane (ik)
Bound receptor (ij)
Free receptor (ij)
PIN internalization (ij)
Bound receptor (ik)
Free receptor (ik)
PIN internalization (ik)

Supplementary Figure 2. Model sensitivity with respect to abundance of extracellular auxin receptors.

(A-D) *In silico* 'WT' control simulation **-** Model simulations on the file of cells (A) and on the cellular grid (B) showed PIN polarization and canalization of auxin flow from an auxin source towards a distal auxin sink. The amount of receptors in the intercellular pools was: R_T = 100 (virtually the same as control simulation presented in Supplementary Figure 1A-D). **(E-H)** Model simulations on the file of cells (E) and on the cellular grid (F) are presented for R_T = 10000. The predicted vascular pattern by model simulation had dropped auxin concentrations (G) presumably due to high levels of extracellular auxin signaling (H), more PINs at the plasma membranes and thus more PIN-dependent auxin transport in the tissue (G). Note that steady-state values of PI and SA were slightly increased (G, H) compared to those in control simulation (C, D) **(I-L)** Model simulations on the file of cells (I) and on the cellular grid (J) are presented for R_T = 1. Here, R_T parameter was significantly reduced which was reflected in over-accumulation of auxin in the cell (K) and the high PIN internalization rates (L). Note that both PI and SA were practically 0. However, the reduction of effective rate of PIN internalization ($\mu = 1\ s^{-1}$) by a 10-fold was sufficient to reestablish differential auxin signaling (increased SA) **(O, P)**, trigger PIN polarization (PI > 0) and reproduce vein pattern **(M, N).** These findings indicate parameter μ is limiting parameter for PIN recycling. Inset of parameter μ allows in our model to increase or decrease PIN levels at the plasma membrane to modulate a sensitivity of feedback mechanism to the amount of extracellular receptors available in the intracellular pool.

Polarization Index (PI) and Signaling Asymmetry (SA) are introduced in Figure 2. For symbols and color code, see Figures 2E and Supplementary Figure 1N.

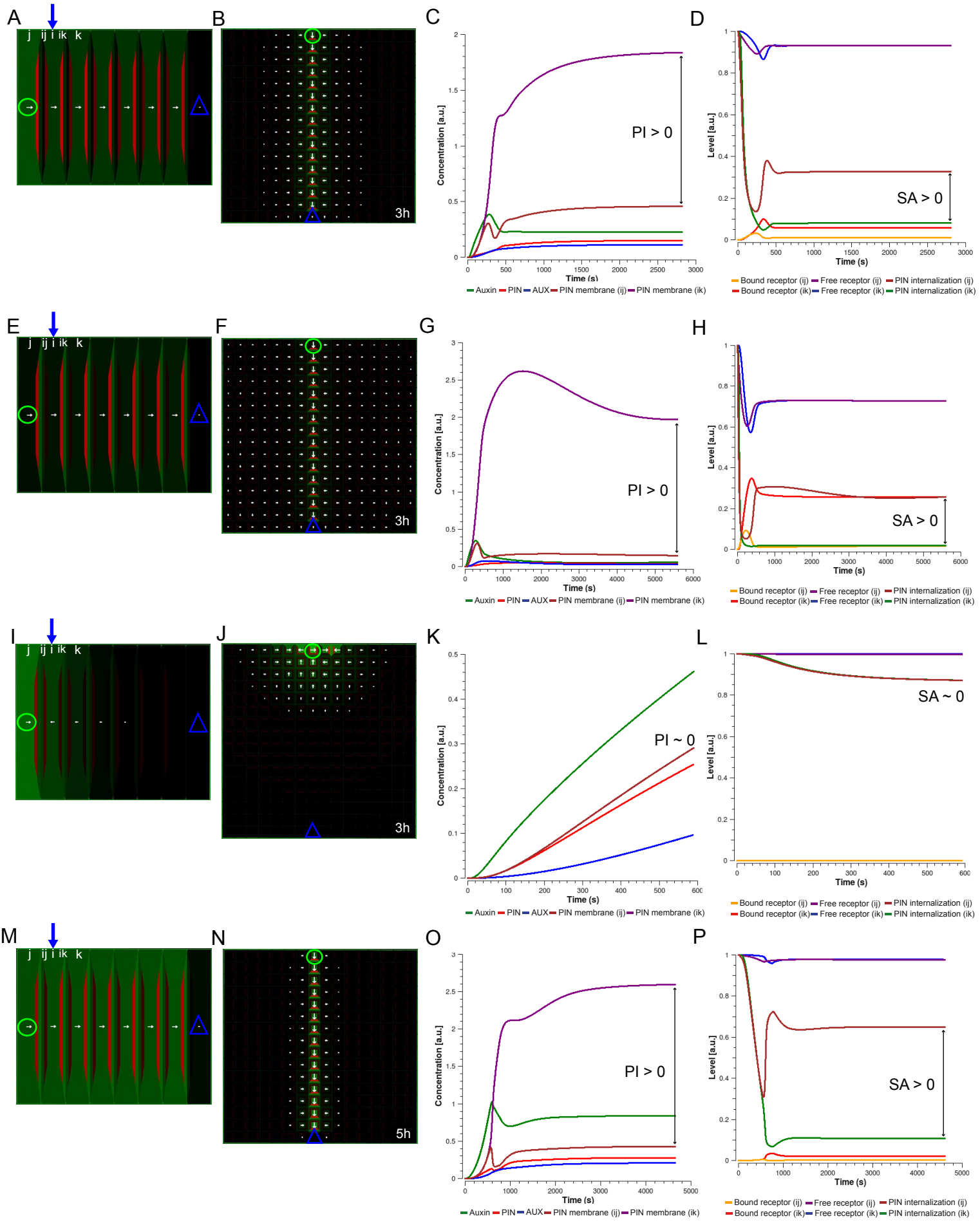
A
B
C
D
E
F
G
H
I
J
K
L
M
N
O
P
j ij i ik k
3h
5h
PI > 0
PI ~ 0
SA > 0
SA ~ 0
Concentration [a.u.]
Level [a.u.]
Time (s)
Auxin
PIN
AUX
PIN membrane (ij)
PIN membrane (ik)
Bound receptor (ij)
Free receptor (ij)
PIN internalization (ij)
Bound receptor (ik)
Free receptor (ik)
PIN internalization (ik)

Supplementary Figure 3. Model sensitivity with respect to extracellular receptor recycling. **(A-D)** *In silico* 'WT' control simulation - Model simulations on the file of cells (A) and on the cellular grid (B) reproduced PIN polarization and canalization of auxin flow from an auxin source towards a distal auxin sink. The dissociation constant of extracellular receptor (represented by the ratio between forward and backward rates of receptor cycling, equation 14) was: K_D = 1 μM (virtually the same as control simulation presented in Supplementary Figure 1A-D). **(E-H)** Model simulations on the file of cells (E) and on the cellular grid (F) are presented for K_D = 0.1 μM. This model simulation predicted the vascular pattern with lower auxin concentrations in the channel due to appearance of more PINs at the plasma membrane and higher auxin transport in the cells (G). However, the appearance of low auxin concentrations in this model simulation resulted in saturated auxin signaling (higher SA (H) compared to control simulation (D)). Also a strong PIN polarity was observed (increased PI) (G). **(I-L)** Model simulations on the file of cells (I) and on the cellular grid (J) are presented for K_D = 10 μM. Due to low affinity rate (high K_D) receptor-based auxin signaling was partially blocked (SA ~ 0) (L) and no PIN polarization (PI ~ 0) was predicted by the model (K). Interestingly, a 10-fold decrease of diffusion of auxin in the apoplast **(M-P)** resulted in increased SA (P) and strong PIN polarization (increased PI) yet enough to canalise auxin flow (M, N). Notably, the time point at the initiation of PIN polarization (for PI > 0) was delayed (~500s, O, P) compared to that in the control simulation (~250s, C, D). This finding implicates that auxin binding to extracellular receptor should occur fast (K_D < 10 μM) to balance the effect of free auxin diffusion in the cell wall. Interestingly, the putative auxin binding protein (ABP1) - a candidate for extracellular auxin receptor, has high affinity and specificity to auxin (K_D ranges from 0.05 μM to 5 μM) for pH of 5.5 [17].

Polarization Index (PI) and Signaling Asymmetry (SA) are introduced in Figure 2. For symbols and color code, see Figures 2E and Supplementary Figure 1N.

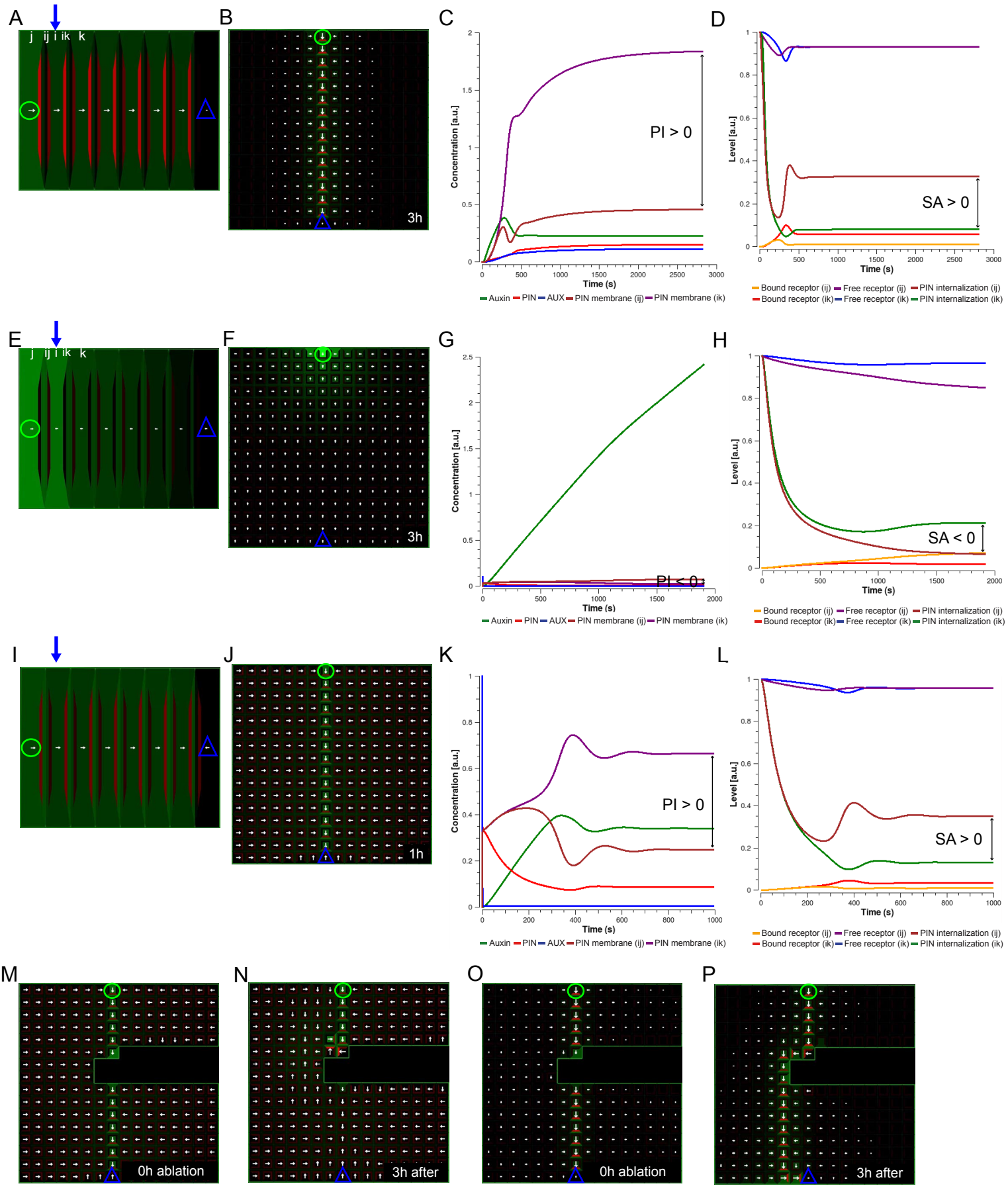
A
j ij i ik k
B
3h
C
Concentration [a.u.]
PI > 0
Time (s)
Auxin PIN AUX PIN membrane (ij) PIN membrane (ik)
D
Level [a.u.]
SA > 0
Time (s)
Bound receptor (ij) Free receptor (ij) PIN internalization (ij)
Bound receptor (ik) Free receptor (ik) PIN internalization (ik)
E
j ij i ik k
F
3h
G
Concentration [a.u.]
PI < 0
Time (s)
Auxin PIN AUX PIN membrane (ij) PIN membrane (ik)
H
Level [a.u.]
SA < 0
Time (s)
Bound receptor (ij) Free receptor (ij) PIN internalization (ij)
Bound receptor (ik) Free receptor (ik) PIN internalization (ik)
I
J
1h
K
Concentration [a.u.]
PI > 0
Time (s)
Auxin PIN AUX PIN membrane (ij) PIN membrane (ik)
L
Level [a.u.]
SA > 0
Time (s)
Bound receptor (ij) Free receptor (ij) PIN internalization (ij)
Bound receptor (ik) Free receptor (ik) PIN internalization (ik)
M
0h ablation
N
3h after
O
0h ablation
P
3h after

Supplementary Figure 4. The role of auxin-dependent carrier expression in vascular patterning and tissue regeneration.

(A-D) *In silico* 'WT' control simulation **-** Model simulations on the file of cells (A) and on the cellular grid (B) predicted PIN polarization and canalization of auxin flow from an auxin source towards a distal auxin sink. The auxin-dependent carrier expression rates were: α_{PIN}=0.1, α_{AUX}=0.1, and carrier degradation terms: δ_{PIN}=0.003, δ_{AUX}=0.003 (equations 5-7, virtually the same as control simulation presented in Supplementary Figure 1A-D). **(E-H)** Simulations on the file of cells (E) and on the cellular grid (F) are presented for the model conditions that do not include auxin-induced carrier expression. Initially, the fixed pool of auxin carriers was assigned to each cell and set at 0.1 a.u. (arbitrary units). Under this condition, auxin canalization could not be reproduced by the ERP model simulations (E, F). The observed values of PI and SA were negative which resulted in the adverse PIN polarization (towards auxin source) in our model simulations (G, H). **(I-L)** Model simulations on the file of cells (I) and on the cellular grid (J) are presented. The amount of auxin carriers in the pool was set at 1 (K, L). The positive values of both PI and SA were associated with PIN polarization from and an auxin source (I, J). Although, the steady-state patterns of PIN polarization were obtained after approx. 16 min (K, L) which was faster than in control simulation (~50 min) (C, D). This results clearly indicate that PIN proteins are important components of the model and thus the sufficient level of PINs (>= 1 a.u.) has to be associated with each cell when carrier expression is turned off. **(M-P)** Simulations of tissue regeneration on the regular cellular grid. (M, N) Fixed pool of carriers in each cell was set at 1 a.u. and no regeneration of vascular pattern was observed (N). (O, P) 'WT' control simulation – model with auxin-induced carrier expression and fixed carrier degradation predicts dynamic re-polarization of cells in direct surrounding of ablated region, down regulation of PINs below the wound and consequently vein regeneration (P).

These results of the model simulations suggest that both PIN degradation and a dynamic regulation of PIN expression by auxin are necessary to narrow down PIN expression domains below the ablated region, and subsequent for *de novo* polarization of PINs (P).

Polarization Index (PI) and Signaling Asymmetry (SA) are introduced in Figure 2. For symbols and color code, see Figures 2E and Supplementary Figure 1N.

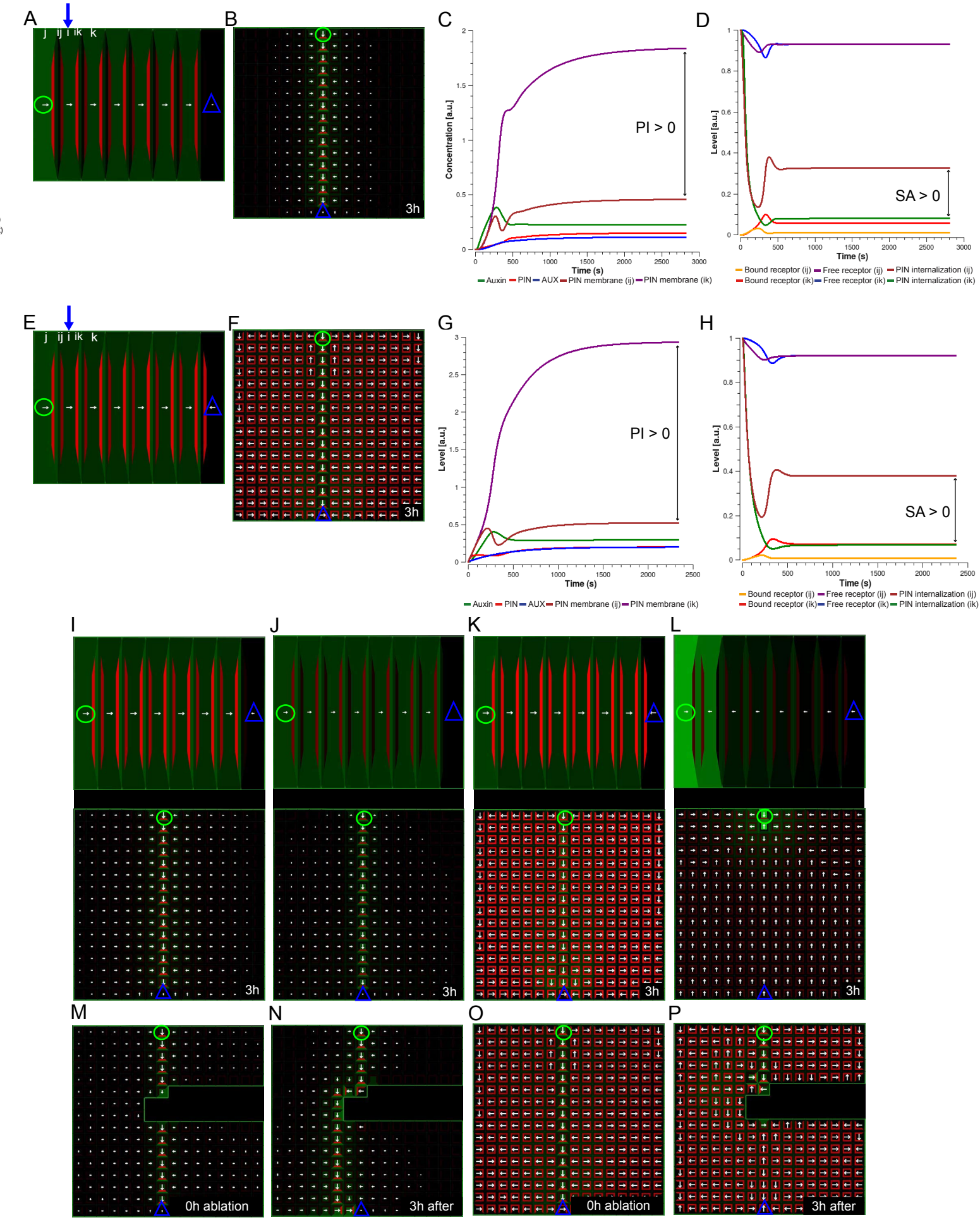
A
j ij i ik k
B
3h
C
PI > 0
Concentration [a.u.]
Time (s)
Auxin PIN AUX PIN membrane (ij) PIN membrane (ik)
D
SA > 0
Level [a.u.]
Time (s)
Bound receptor (ij) Free receptor (ij) PIN internalization (ij)
Bound receptor (ik) Free receptor (ik) PIN internalization (ik)
E
j ij i ik k
F
3h
G
PI > 0
Level [a.u.]
Time (s)
Auxin PIN AUX PIN membrane (ij) PIN membrane (ik)
H
SA > 0
Level [a.u.]
Time (s)
Bound receptor (ij) Free receptor (ij) PIN internalization (ij)
Bound receptor (ik) Free receptor (ik) PIN internalization (ik)
I
3h
J
3h
K
3h
L
3h
M
0h ablation
N
3h after
O
0h ablation
P
3h after

Supplementary Figure 5. Auxin-dependent *versus* auxin-independent carrier expression in vascular patterning and tissue regeneration.

(A-D) *In silico* 'WT' control simulation **-** Model simulations on the file of cells (A) and on the cellular grid (B) predicted PIN polarization and canalization of auxin flow from an auxin source towards a distal auxin sink. The auxin-dependent carrier expression rates were: α_{PIN}=0.1, α_{AUX}=0.1, and carrier degradation terms: δ_{PIN}=0.003, δ_{AUX}=0.003 (equations 5-7, virtually the same as control simulation presented in Supplementary Figure 1A-D). **(E-H)** Model simulations on the file of cells (E) and on the cellular grid (F) are presented for the model with an auxin-independent carrier expression. The rates of fixed carrier expression were: α_{PIN}=0.01, α_{AUX}=0.01, and carrier degradation terms: δ_{PIN}=0.003, δ_{AUX}=0.003. The ERP model predicted the canalization of auxin flow and basal PIN polarization in pro-vascular cells (E, F). Note that PI and SA were slightly increased (G, H) compared to those in control simulation (C, D) presumably due to higher PIN signal at the plasma membrane of each cell. Notably, this model simulation predicted the adverse PIN polarization in the cells that surrounded pro-vascular channel, and only broad, uniform and strong PIN expression was observed in the whole tissue (F). **(I-J)** Simulations on the file of cells and on the cellular grid for the ERP model with auxin-dependent carrier expression rates that were: α_{PIN}=1, α_{AUX}=1 (I) and α_{PIN}=0.01, α_{AUX}=0.01 (J). **(K-L)** Model simulations on the file of cells and on the cellular grid with fixed carrier expression rates: α_{PIN}=0.1, α_{AUX}=0.1 (K) and α_{PIN}=0.001, α_{AUX}=0.001 (L) are presented. Note that low levels of carrier expression in the model resulted in patterning defects (L). **(M-P)** 'WT' control simulation – the model with an auxin-induced carrier expression allows for dynamic re-polarization of cells in direct surrounding of ablated region, down regulation of PINs below the wound and consequently vein regeneration (M, N). The model with fixed carrier expression (α_{PIN}=0.01, α_{AUX}=0.01) was not able to reproduce PIN polarization during vein regeneration (O, P).

In agreement with results presented in Supplementary Figure 4, these model simulations demonstrated the importance of auxin-dependent regulation of PIN expression for generating realistic, narrowed and flexible PIN polarization patterns during auxin canalization and vascular regeneration.

Polarization Index (PI) and Signaling Asymmetry (SA) are introduced in Figure 2. For symbols and color code, see Figures 2E and Supplementary Figure 1N.

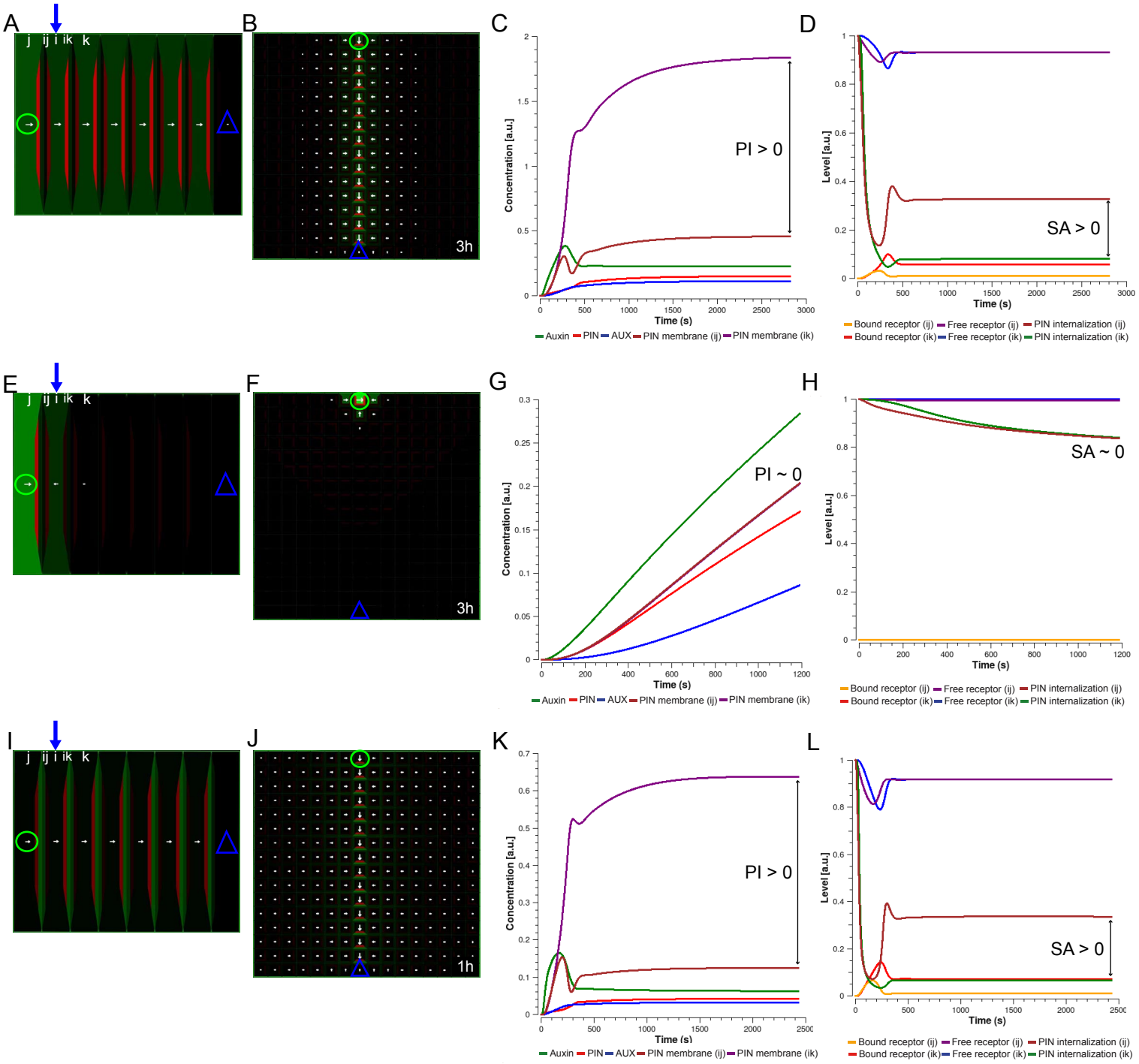
A
j ij i ik k
B
3h
C
Concentration [a.u.]
PI > 0
Time (s)
Auxin PIN AUX PIN membrane (ij) PIN membrane (ik)
D
Level [a.u.]
SA > 0
Time (s)
Bound receptor (ij) Free receptor (ij) PIN internalization (ij)
Bound receptor (ik) Free receptor (ik) PIN internalization (ik)
E
j ij i ik k
F
3h
G
Concentration [a.u.]
PI ~ 0
Time (s)
Auxin PIN AUX PIN membrane (ij) PIN membrane (ik)
H
Level [a.u.]
SA ~ 0
Time (s)
Bound receptor (ij) Free receptor (ij) PIN internalization (ij)
Bound receptor (ik) Free receptor (ik) PIN internalization (ik)
I
j ij i ik k
J
1h
K
Concentration [a.u.]
PI > 0
Time (s)
Auxin PIN AUX PIN membrane (ij) PIN membrane (ik)
L
Level [a.u.]
SA > 0
Time (s)
Bound receptor (ij) Free receptor (ij) PIN internalization (ij)
Bound receptor (ik) Free receptor (ik) PIN internalization (ik)

Supplementary Figure 6. Model robustness with respect to the efficiency of PIN-dependent auxin transport.

(A-D) 'WT' control simulation **-** Model simulations on the file of cells (A) and on the cellular grid (B) showed PIN polarization and canalization of auxin flow from an auxin source towards a distal auxin sink. The permeability of PIN-dependent transport (p_{PIN}) was set at 30 μms^{-1} (virtually the same as control simulation presented in Supplementary Figure 1A-D). **(E-H)** Model simulations on the file of cells (E) and on the cellular grid (F) are presented for parameter p_{PIN}=1 μms^{-1} which mimic *pin* mutants (practically the lack of PIN-dependent transport). In this simulation, the canalization of auxin flow did not occur (E, F). Moreover, model predicted accumulation of auxin in the tracked cell (G) which resulted in the lack of PIN polarization (PI ~ 0) (G) and no visible asymmetry in extracellular auxin signaling (SA ~ 0) (H). **(I-L)**. Model simulations on the file of cells (I) and on the cellular grid (J) are presented for parameter p_{PIN}=300. In this case the capacity of PIN-dependent auxin transport (p_{PIN}) was set a 10-fold higher than that in control simulation (A-D). No qualitative change of model behavior was observed (K, L) compared to control simulation (C, D). Additionally, auxin concentrations were lower in the channel (I, J) than those reported in the control simulation (A, B). These model simulations suggest that the capacity of PIN-dependent auxin transport (p_{PIN}) is crucial parameter for the model to reproduce venation patterning and its inset should be higher than the weak "background" permeability of 1 μms^{-1} (E, H).

Polarization Index (PI) and Signaling Asymmetry (SA) are introduced in Figure 2. For symbols and color code, see Figures 2E and Supplementary Figure 1N.

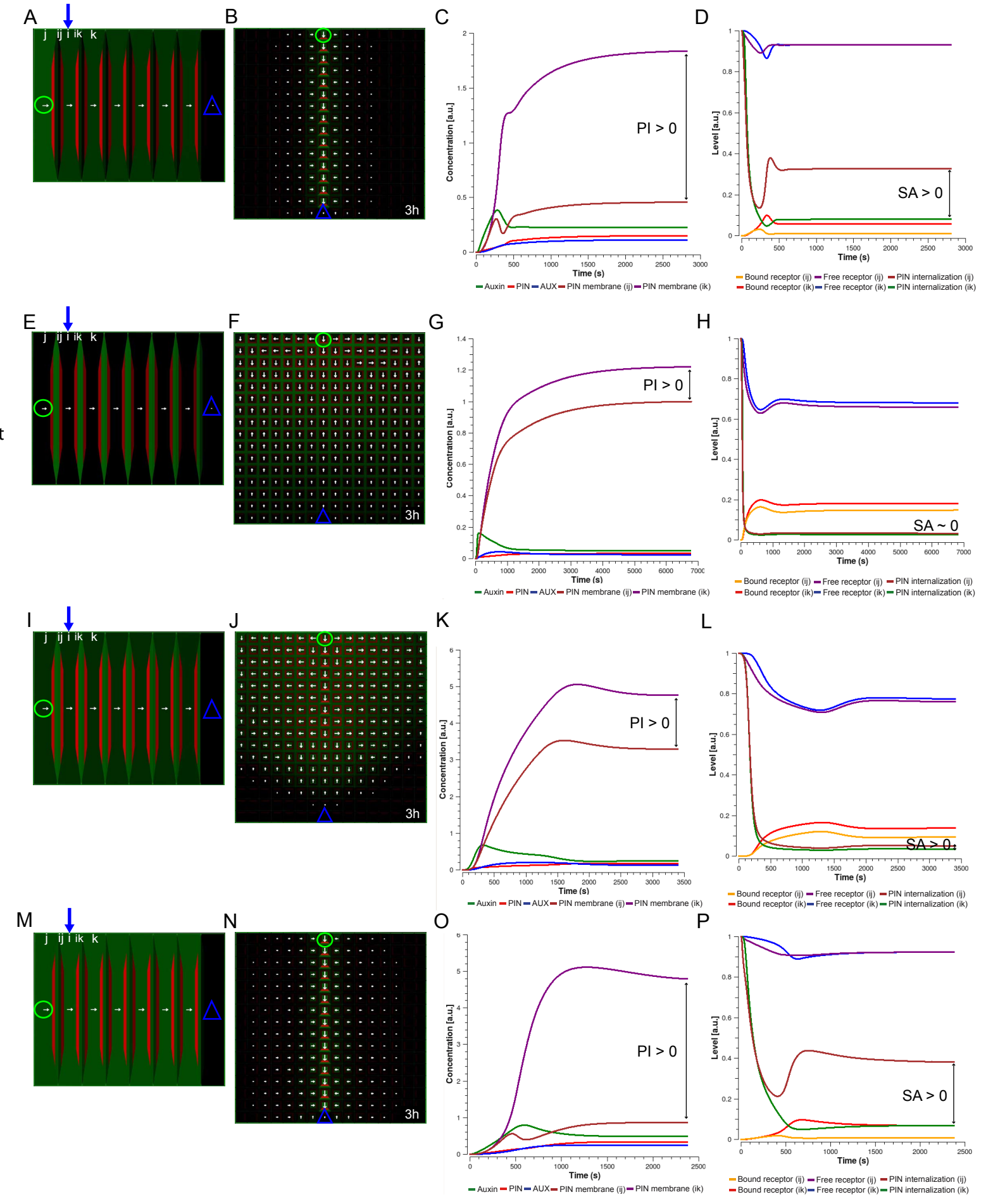
A
B
C
D
E
F
G
H
I
J
K
L
M
N
O
P
j ij i ik k
3h
PI > 0
SA > 0
SA ~ 0
Concentration [a.u.]
Level [a.u.]
Time (s)
Auxin PIN AUX PIN membrane (ij) PIN membrane (ik)
Bound receptor (ij) Free receptor (ij) PIN internalization (ij)
Bound receptor (ik) Free receptor (ik) PIN internalization (ik)

Supplementary Figure 7. Model sensitivity with respect to the efficiency of AUX/LAX-dependent auxin transport.

(A-D) 'WT' control simulation **-** Model simulations on the file of cells (A) and on the cellular grid (B) showed PIN polarization and canalization of auxin flow from an auxin source towards a distal auxin sink. The permeability of AUX/LAX-dependent transport (p_{AUX}) was set at 30 μms^{-1} (virtually the same as control simulation presented in Supplementary Figure 1A-D). **(e-h)** Model simulations on the file of cells (E) and on the cellular grid (F) are reported for parameter p_{AUX}=1 μms^{-1}. Here, the canalization of auxin flow was not predicted by model simulations as well as strong basal PIN polarization in pro-vascular cells and lateral polarization of surrounding tissues (E, F). A very weak difference in PIN levels between *ik*-th and *ij*-th plasma membranes was established (small PI) (G). However, this weak PIN polarization did not get enhanced and maintained presumably due to a shallow difference in extracellular auxin signaling across the cell wall (SA ~ 0) (H). **(I-L)** Model simulations on the file of cells (I) and on the cellular grid (J) are presented for parameter p_{AUX} set at 1 μms^{-1} and for a 10-fold higher inset of p_{IAAH}. Note that *in silico* AUX/LAX phenotype (E-H) was virtually rescued as predicted by model simulation (I, J). Nevertheless, the basal PIN polarization in the pro-vascular cells was not maintained (small PI) and thus an auxin source did not connect to a distal auxin sink (J). Interestingly, this model simulation predicted no delay in the initiation of PIN polarization (K, L) compared to control simulation (C, D). This suggests that a diffusion-based auxin influx into cell (p_{IAAH}) tends to delay, but does not balance the auxin efflux from cell (K). Consequently, auxin was trapped in the extracellular space in high concentrations and thus no significant asymmetry in extracellular auxin signaling was generated (SA ~ 0) (L). Our model simulations indicate that the contribution of AUX/LAX carriers to the dynamic drainage of auxin from the apoplast is central to the maintenance of basal PIN polarization in the pro-vascular cells and lateral PIN polarization of surrounding tissues (A, B). **(M-P)** Model simulations on the file of cells (M) and on the cellular grid (N) are presented for parameter p_{AUX}=300 μms^{-1}. The capacity of AUX/LAX-dependent auxin transport was a 10-fold higher than that in control simulation (A-D). Model predicted that auxin efflux from the cell is balanced by active AUX/LAX influx resulting in increased PI (O) and increased SA (P).

Polarization Index (PI) and Signaling Asymmetry (SA) are introduced in Figure 2. For symbols and color code, see Figures 2E and Supplementary Figure 1N.

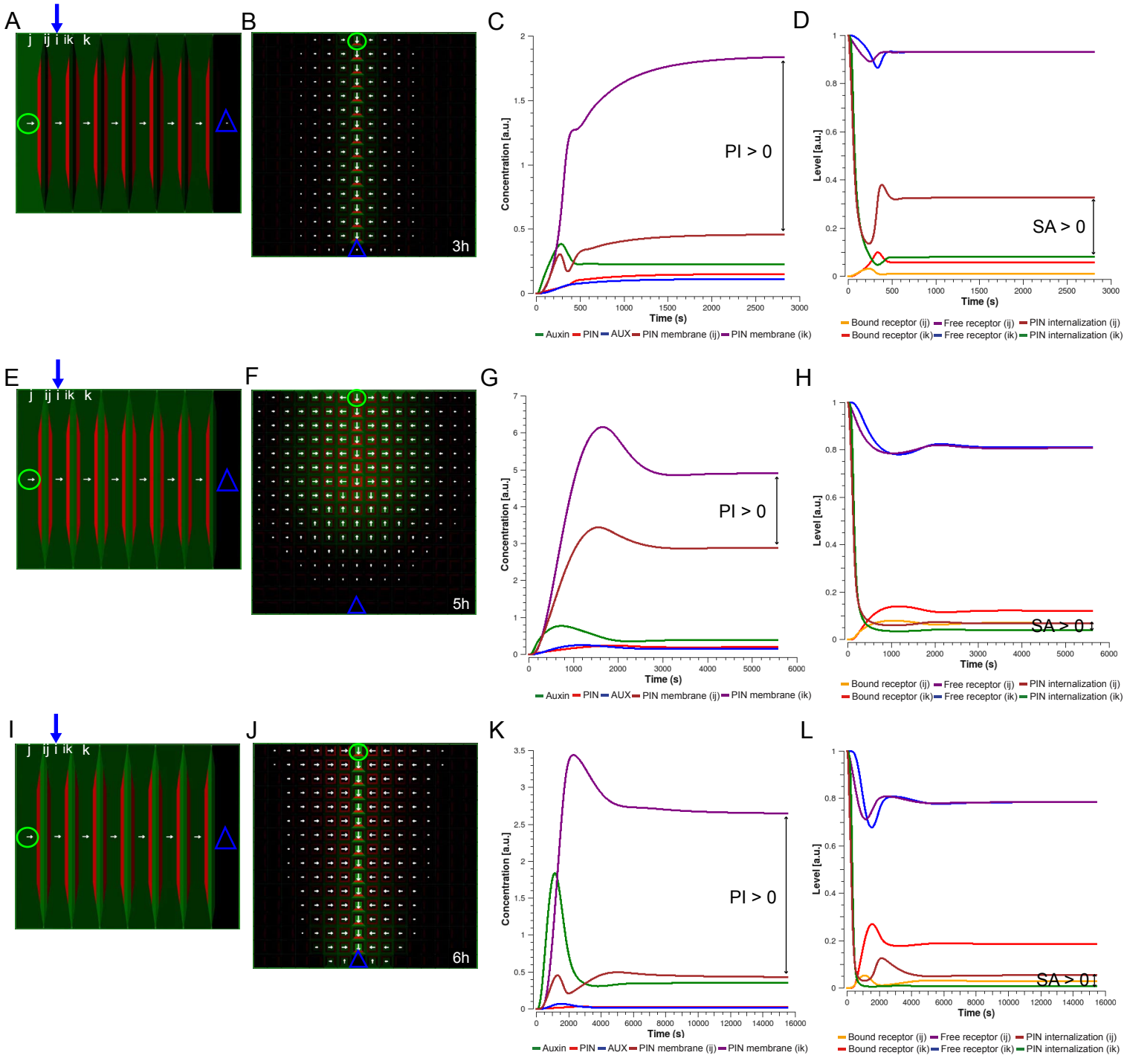
A
j ij i ik k
B
3h
C
Concentration [a.u.]
PI > 0
Time (s)
Auxin PIN AUX PIN membrane (ij) PIN membrane (ik)
D
Level [a.u.]
SA > 0
Time (s)
Bound receptor (ij) Free receptor (ij) PIN internalization (ij)
Bound receptor (ik) Free receptor (ik) PIN internalization (ik)
E
j ij i ik k
F
5h
G
Concentration [a.u.]
PI > 0
Time (s)
Auxin PIN AUX PIN membrane (ij) PIN membrane (ik)
H
Level [a.u.]
SA > 0
Time (s)
Bound receptor (ij) Free receptor (ij) PIN internalization (ij)
Bound receptor (ik) Free receptor (ik) PIN internalization (ik)
I
j ij i ik k
J
6h
K
Concentration [a.u.]
PI > 0
Time (s)
Auxin PIN AUX PIN membrane (ij) PIN membrane (ik)
L
Level [a.u.]
SA > 0
Time (s)
Bound receptor (ij) Free receptor (ij) PIN internalization (ij)
Bound receptor (ik) Free receptor (ik) PIN internalization (ik)

Supplementary Figure 8. Model sensitivity with respect to the speed of polar auxin transport.

(A-D) 'WT' control simulation **-** Model simulations on the file of cells (A) and on the cellular grid (B) showed PIN polarization and canalization of auxin flow from an auxin source towards a distal auxin sink. The saturation of polar auxin transport (k_t) was set at 1 μM (virtually the same as control simulations presented in Supplementary Figure 1A-D). **(E-H)** Model simulations on the file of cells (E) and on the cellular grid (F) are presented for parameter k_t=10 μM. The initiation of PIN polarization was observed (PI > 0) (G), however, no significant difference in extracellular auxin signaling was reported (low SA) (H). The model simulations predicted a transient basal PIN polarization in pro-vascular cells and no lateral polarization of surrounding tissues (E, F). In this case the low capacity of polar auxin transport provided no means to counteract apoplastic auxin diffusion and consequently, PIN polarization associated with the positive value of PI could not be sufficiently maintained (G, H). **(I-L)** Model simulations on the file of cells (I) and on the cellular grid (J) are presented for parameter k_t=10 μM, and a 10-fold decrease of auxin diffusion in the apoplast (D_a) compared to that used in control simulations (D_a = 100 $\mu m^2 s^{-1}$). (I, J) Model predicted virtual rescue of *in silico* phenotype (E-H). Notably, the simulation demonstrated a transient maximum of PI associated with PIN polarization that was a 10-fold stronger (K) than that observed in control simulation (C). Similarly, this reduction in apoplastic diffusion (D_a) in our model resulted in an increase of SA (L). This indicates that the speed of carrier-dependent auxin transport system has to be comparable or faster than passive movement of auxin within the cell wall.

Polarization Index (PI) and Signaling Asymmetry (SA) are introduced in Figure 2. For symbols and color code, see Figures 2E and Supplementary Figure 1N.

A

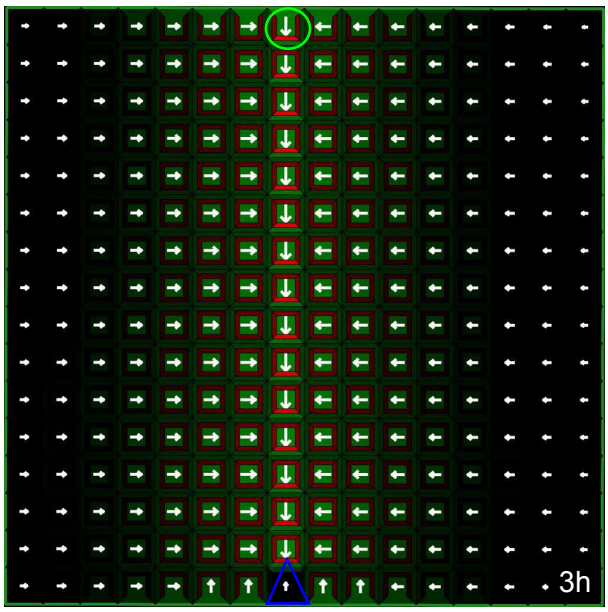

B

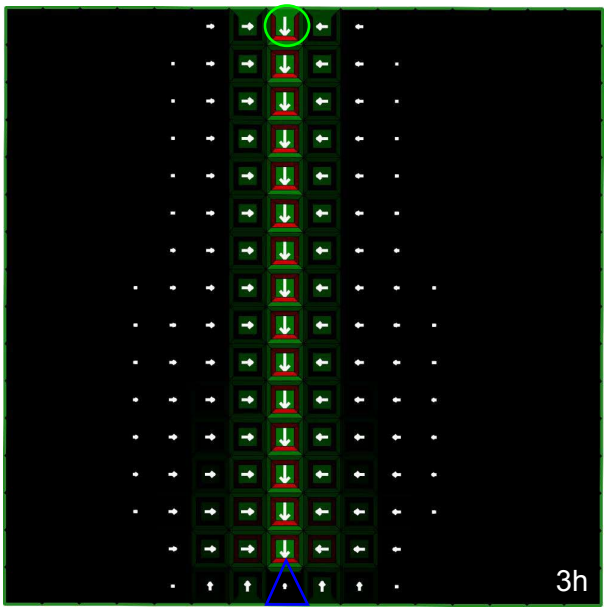

C

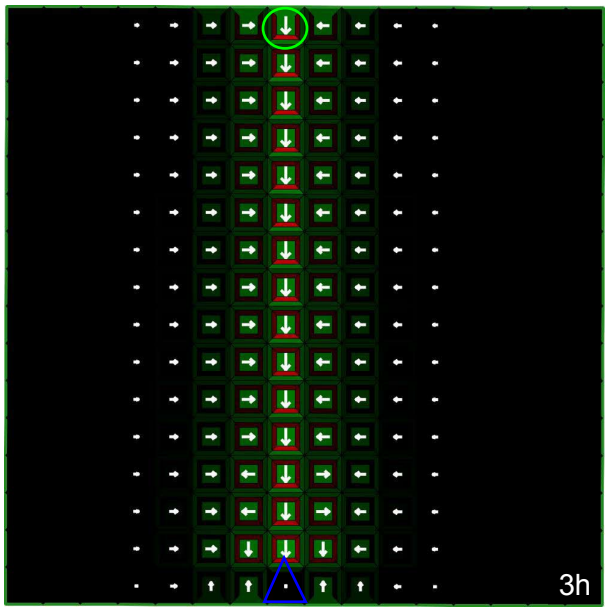

D

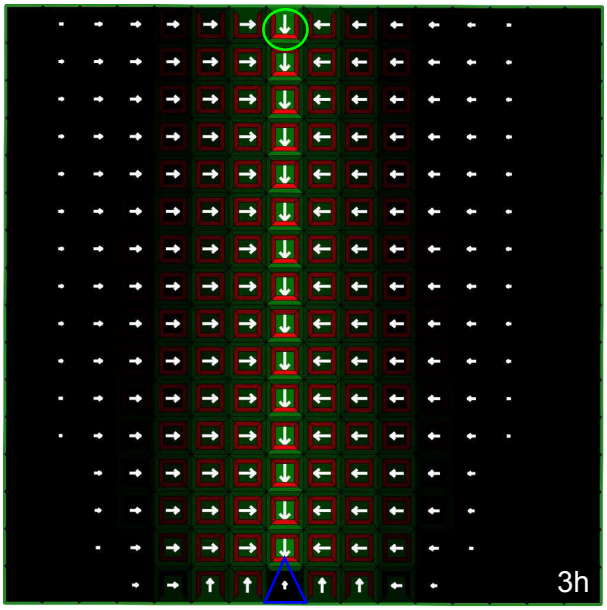

Supplementary Figure 9. Model robustness with respect to diffusion and permeability rates.

(A) PIN polarity and auxin distribution patterns for a 5-fold increase of apoplastic auxin diffusion (D_a) that was originally set at 100 $\mu m^2 s^{-1}$. **(B)** A sharp auxin distribution pattern was observed in the model simulation with a 5-fold decrease of D_a. The ERP model with the values of apoplastic auxin diffusion from range of 10 $\mu m^2 s^{-1}$ up to 500 $\mu m^2 s^{-1}$ which covers the variety of measurement of apoplastic auxin diffusion in plants [11]-[13]. **(C)** A 5-fold increase in the total membrane permeability values (p_{PIN} and p_{AUX}) had no visible impact on PIN polarization and the canalization of auxin flow. **(D)** Cell polarity and auxin distribution patterns in model simulation with a 5-fold decrease in the total permeability values: $p_{PIN}=p_{AUX}=6$ $\mu m s^{-1}$.

For symbols and color code, see Figures 2E and Supplementary Figure 1N.

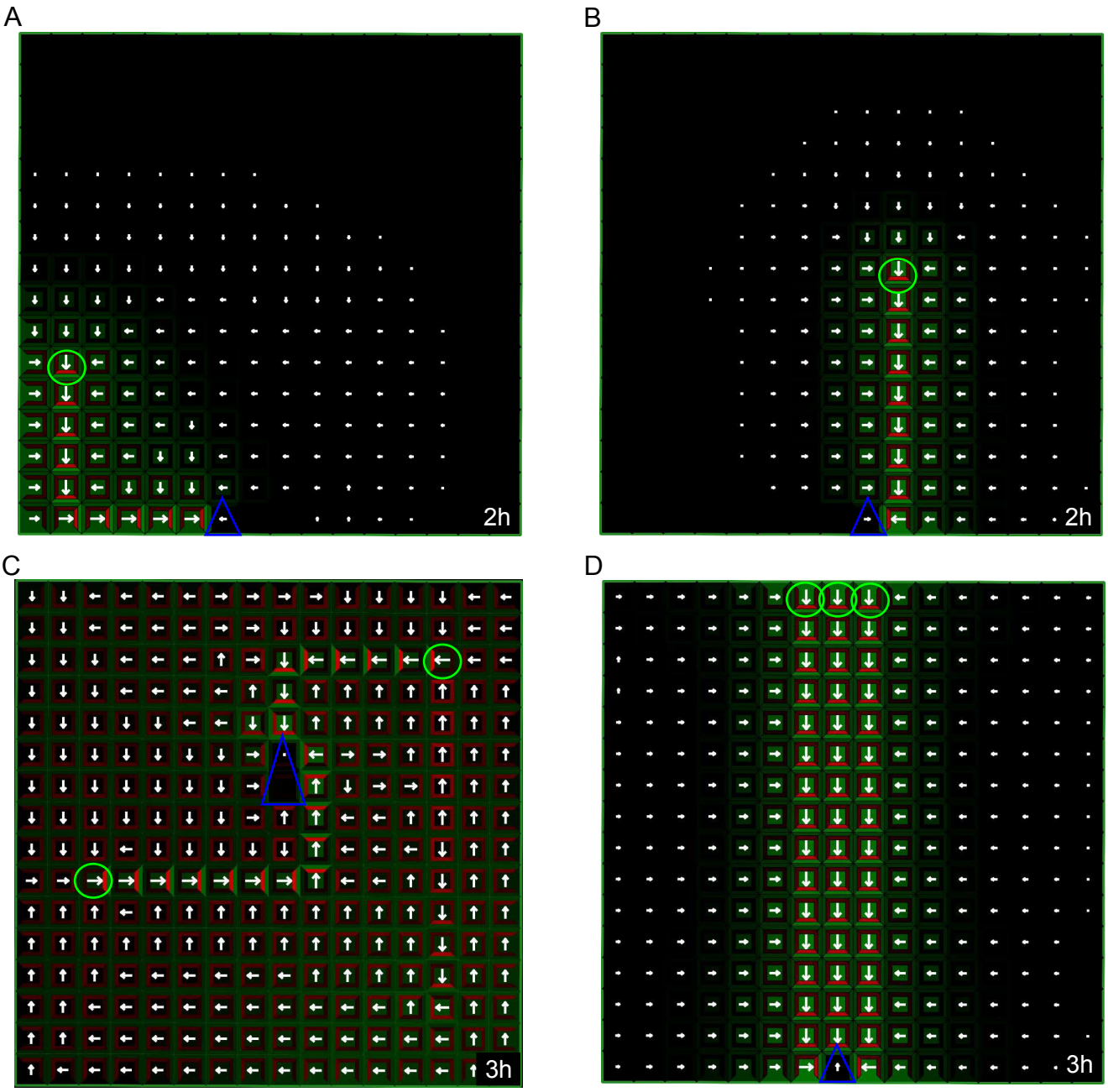
A
2h
B
2h
C
3h
D
3h

Supplementary Figure 10. **Model sensitivity with respect to altered boundary conditions.**
(A) Model simulation of auxin canalization on regular grid with an auxin source that was placed against the boundary. The strength of auxin source was set at 0.001 $\mu M\ \mu m^{-2}\ s^{-1}$. Auxin canalization was observed in this ERP model simulation (A). Interestingly, the predicted auxin channel was not stringent to tissue boundary compared with the observations from predictions of classical canalization models suggesting that the ERP model faithfully and robustly reproduces auxin canalization patterns. (**B)** Auxin canalization on the regular grid predicted by the ERP mechanism with randomly chosen spot of the auxin biosynthesis. **(C)** The ERP model provides the robust sink finder mechanism for auxin canalization. An auxin sink was set at the random position on the cellular grid and two, equivalent in strength auxin sources ($0.001\ \mu M\ \mu m^{-2}\ s^{-1}$) were introduced at the same time on the grid tissue layout. The shortest path from each auxin source to an auxin sink was robustly found in the ERP model simulation (C).
(D) The widening of auxin channel in the ERP model simulation. The single-cell auxin source located in the center of the top cell layer of a grid tissue layout was extended to the two adjacent cells which resulted in the formation of broad auxin channel (D).
For symbols and color code, see Figures 2E and Supplementary Figure 1N.

A

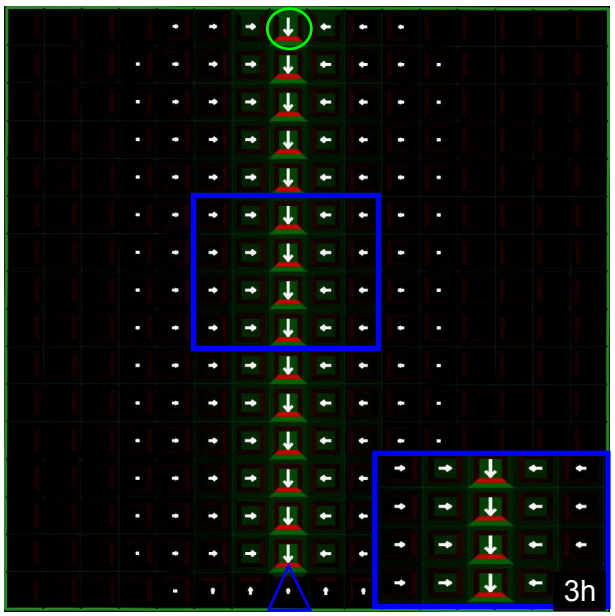

B

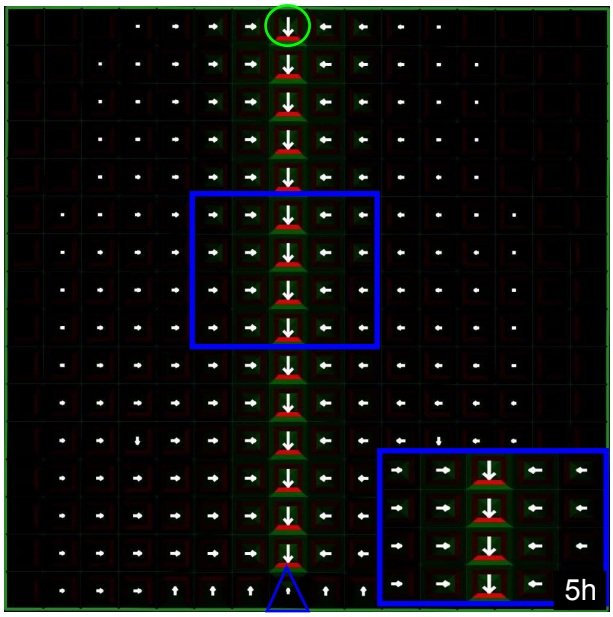

C

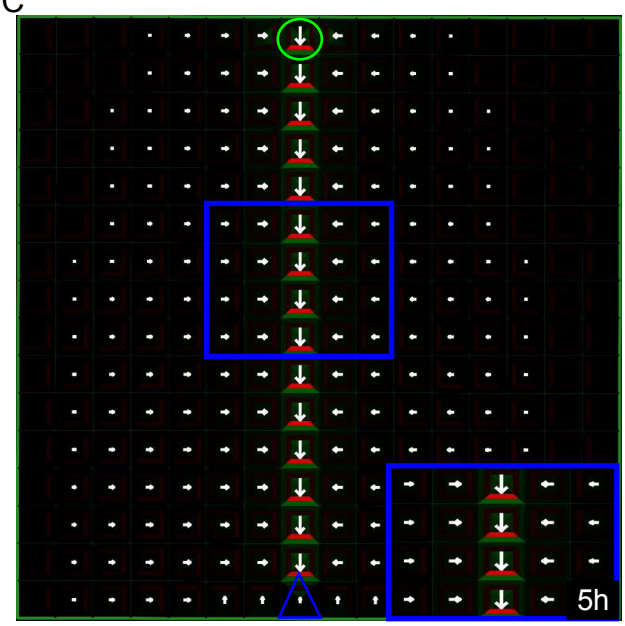

D

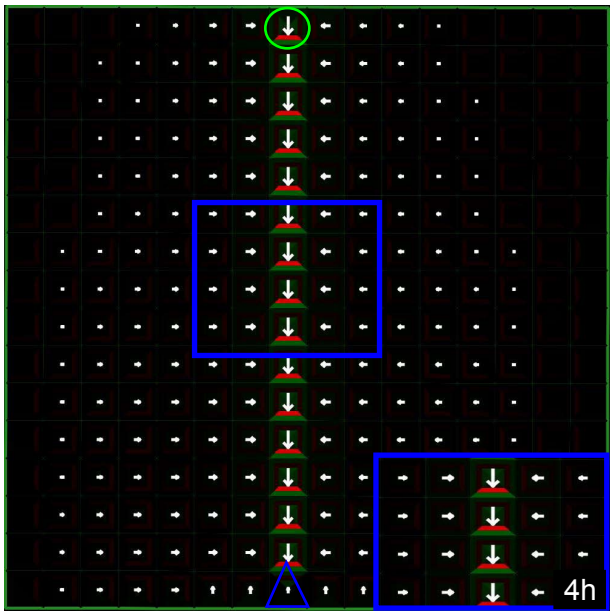

E

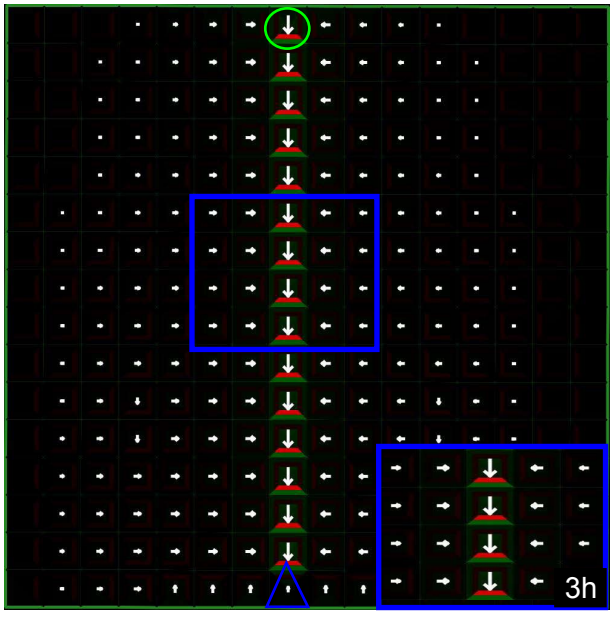

F

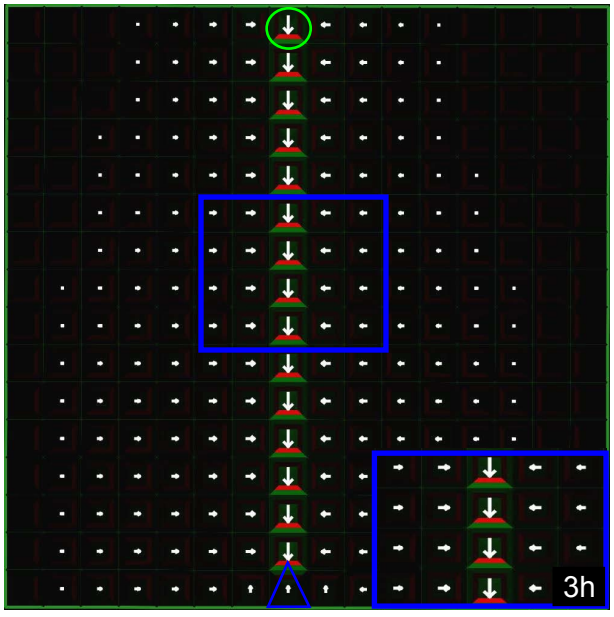

Supplementary Figure 11. **The ERP model with intracellular auxin diffusion.**

(A) Model simulations on the file of cells (A) and on the cellular grid (B) showed PIN polarization and canalization of auxin flow from an auxin source towards a distal auxin sink. Each cell is represented by a rectangular square with the mean auxin concentration in the cytoplasm (A) (the model inset was the same as simulation presented in Figure 3A and 3B). **(B)** The square box representing one cell was divided in four identical intracellular compartments and each component associated with the one side of the cell and the cell center. Here our model additionally integrated an intracellular auxin diffusion between these intracellular compartments that was described by Fick's law:

$$J_{1->2} = -D \cdot \frac{c_1 - c_2}{L}$$

where $J_{1->2}$ is the net flux from intracellular compartment 1 to intracellular compartment 2, c_j is the concentration of intracellular auxin in compartment j for j=1, 2, and D is the diffusion coefficient of auxin in the cell, and L is a distance between the compartments. **(B)** The diffusion coefficient D was set at 10 $\mu m^2 s^{-1}$, **(C)** D = 50 $\mu m^2 s^{-1}$, **(D)** D = 100 $\mu m^2 s^{-1}$, **(E)** D = 300 $\mu m^2 s^{-1}$, **(F)** D = 600 $\mu m^2 s^{-1}$. These model simulations that include intracellular auxin diffusion were performed for a wide range of diffusion rates (B-F) and were yielded qualitatively similar predictions as the control simulations with no intracellular auxin diffusion (A).

Polarization Index (PI) and Signaling Asymmetry (SA) are introduced in Figure 2. For symbols and color code, see Figures 2E and Supplementary Figure 1N.

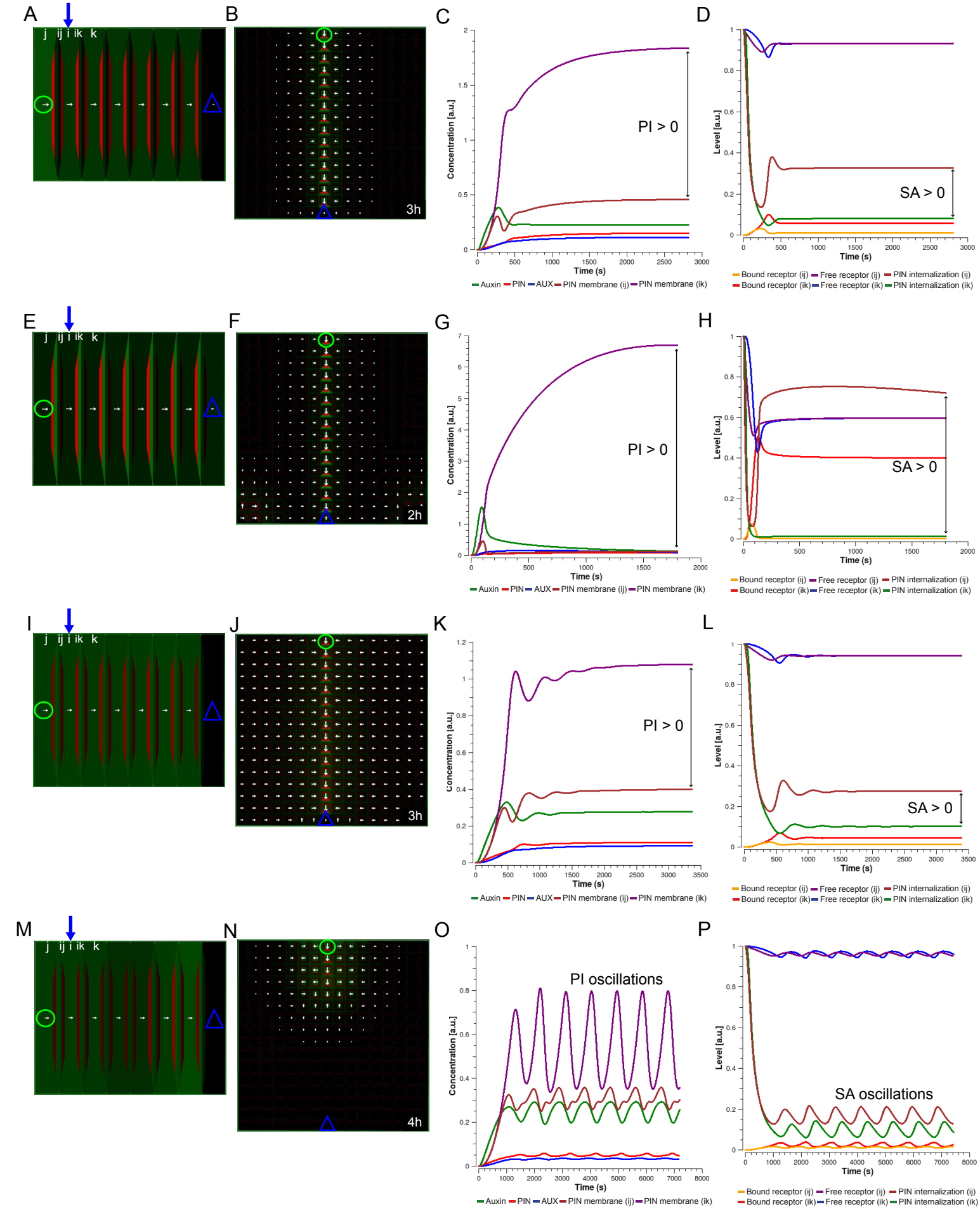
A
B
C
D
j ij i ik k
3h
PI > 0
SA > 0
Concentration [a.u.]
Level [a.u.]
Time (s)
Auxin PIN AUX PIN membrane (ij) PIN membrane (ik)
Bound receptor (ij) Free receptor (ij) PIN internalization (ij)
Bound receptor (ik) Free receptor (ik) PIN internalization (ik)
E
F
G
H
2h
I
J
K
L
M
N
O
P
4h
PI oscillations
SA oscillations

Supplementary Figure 12. Auxin concentration is a main polarizing signal.

(A-D) 'WT' control simulation **-** Model simulations on the file of cells (A) and on the cellular grid (B) predicted PIN polarization and canalization of auxin flow from an auxin source towards a distal auxin sink. The auxin source was set to 0.001 $\mu M\ \mu m^{-2}\ s^{-1}$ (virtually the same as control simulation presented in Supplementary Figure 1A-D). **(E-H).** Model simulations on the file of cells (E) and on the cellular grid (F) with auxin source set to 0.01 $\mu M\ \mu m^{-2}\ s^{-1}$ and a distal auxin sink are presented. The auxin concentration threshold sufficient causing increase of the PI was reached nearly two times faster (G) compared to that presented in control simulation (C). Notably, the model predicted a steep difference in extracellular auxin signaling on both sides of *i*-th cell that was associated with the high positive value of SA (H). The PIN levels on *ik*-th membrane were a 7-fold higher than those on *ij*-th membrane (high PI) (G). **(I-L)** Model simulations on the file of cells (I) and on the cellular grid (J) with auxin source set to 0.0005 $\mu M\ \mu m^{-2}\ s^{-1}$ and a distal auxin sink are presented. The establishment of PIN polarization was delayed (K) in comparison with control simulation (C), by about 100s. This is presumably due to a longer time of auxin accumulation in the cell (K). Interestingly, in the presence of this weak auxin source, our model predicted fluctuations (oscillations) in the steady-state values of chemicals, that were damped over time resulting with stable PIN polarization pattern (K, L). Note that PI and SA – measures of PIN polarization and auxin signaling were also oscillating **(M-P)** Model simulations on the file of cells (M) and on the cellular grid (N) with an auxin source set to 0.0001 $\mu M\ \mu m^{-2}\ s^{-1}$ and a distal auxin sink are presented. In this model simulation, the establishment of PIN polarization was considerably delayed by about 1000 s (O) if compared to predictions from control simulation (C). Also here oscillations of values of PI and SA were observed and those corresponded to similar fluctuations in chemical levels (O, P). In summary, our model predicted unstable PIN polarity resulting in the lack of vascular connection (M, N).

We demonstrated that hot spots of auxin production (auxin sources) mediate the stability of PIN polarization patterns and thus provide means for auxin-regulated processes such as vascular formation/connection (Figures 3, 4, 5, 6A-E) and vascular repulsion (Figure 6I-M).

Polarization Index (PI) and Signaling Asymmetry (SA) are introduced in Figure 2. For symbols and color code, see Figures 2E and Supplementary Figure 1N.

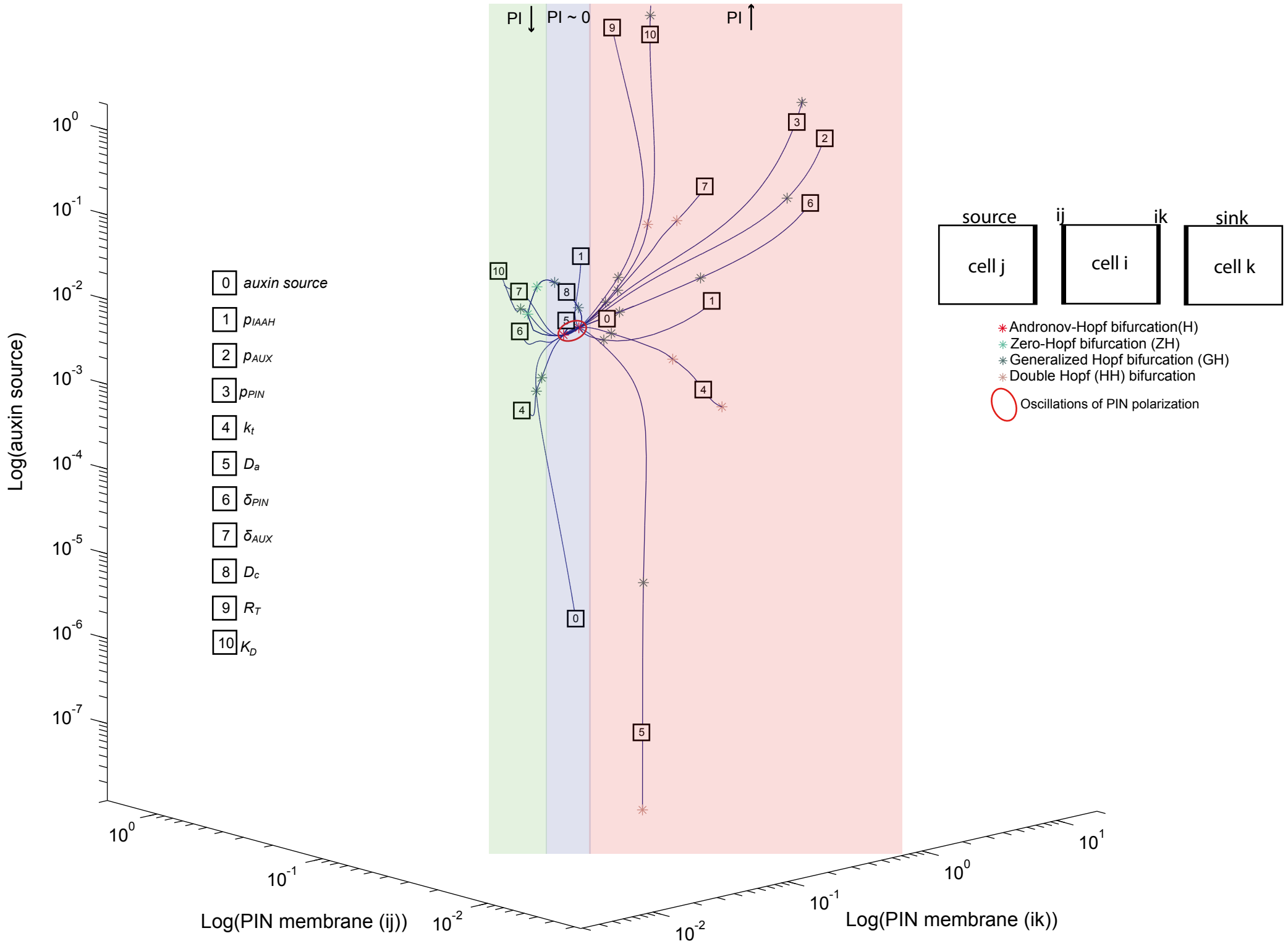
PI ↓
PI ~ 0
PI ↑
Log(auxin source)
Log(PIN membrane (ij))
Log(PIN membrane (ik))
0 auxin source
1 p_{IAAH}
2 p_{AUX}
3 p_{PIN}
4 k_t
5 D_a
6 δ_{PIN}
7 δ_{AUX}
8 D_c
9 R_T
10 K_D
source
ij
ik
sink
cell j
cell i
cell k
Andronov-Hopf bifurcation(H)
Zero-Hopf bifurcation (ZH)
Generalized Hopf bifurcation (GH)
Double Hopf (HH) bifurcation
Oscillations of PIN polarization

Supplementary Figure 13. The evolution of stationary equilibrium under variation of model parameters.

A bifurcation diagram represents the family of stationary solutions for varying source strength (0). Two Hopf-points (H) were detected using numerical continuation of the equilibrium. These points indicate the appearance of supercritical Andronov-Hopf bifurcation with stable limit cycle (first Lapunov coefficients were negative, a pair of purely imaginary eigenvalues). The curve connecting H points corresponds to the parameter regime for which oscillations of PIN polarization occur. The equilibrium curves (1-10) describe the families of stationary solutions for the variation of auxin source strength and one additional model parameter. Note that several additional bifurcations were detected including Generalized Hopf (GH), Zero-Hopf (ZH) (one zero eigenvalue) and Hopf-Hopf (HH) bifurcations. The schematic colorized planes describe three different model behaviors (green, blue, red) which are associated with:

- "Up-the-gradient" PIN polarization (green plane) associated with decreasing Polarization Index (PI)
- Unstable PIN polarization or no PIN polarization (blue plane) when PI is crossing zero.
- "With-the-gradient" PIN polarization (red plane) associated with increasing value of PI.

Each of these model behaviors correspond to different phenomena occurring during canalization of auxin flow in our model simulations that includes vein connection ($PI > 0$), vein repulsion ($PI \sim 0$) and PIN polarization towards an auxin source ($PI < 0$). Polarization Index (PI) is described in Figure 2.

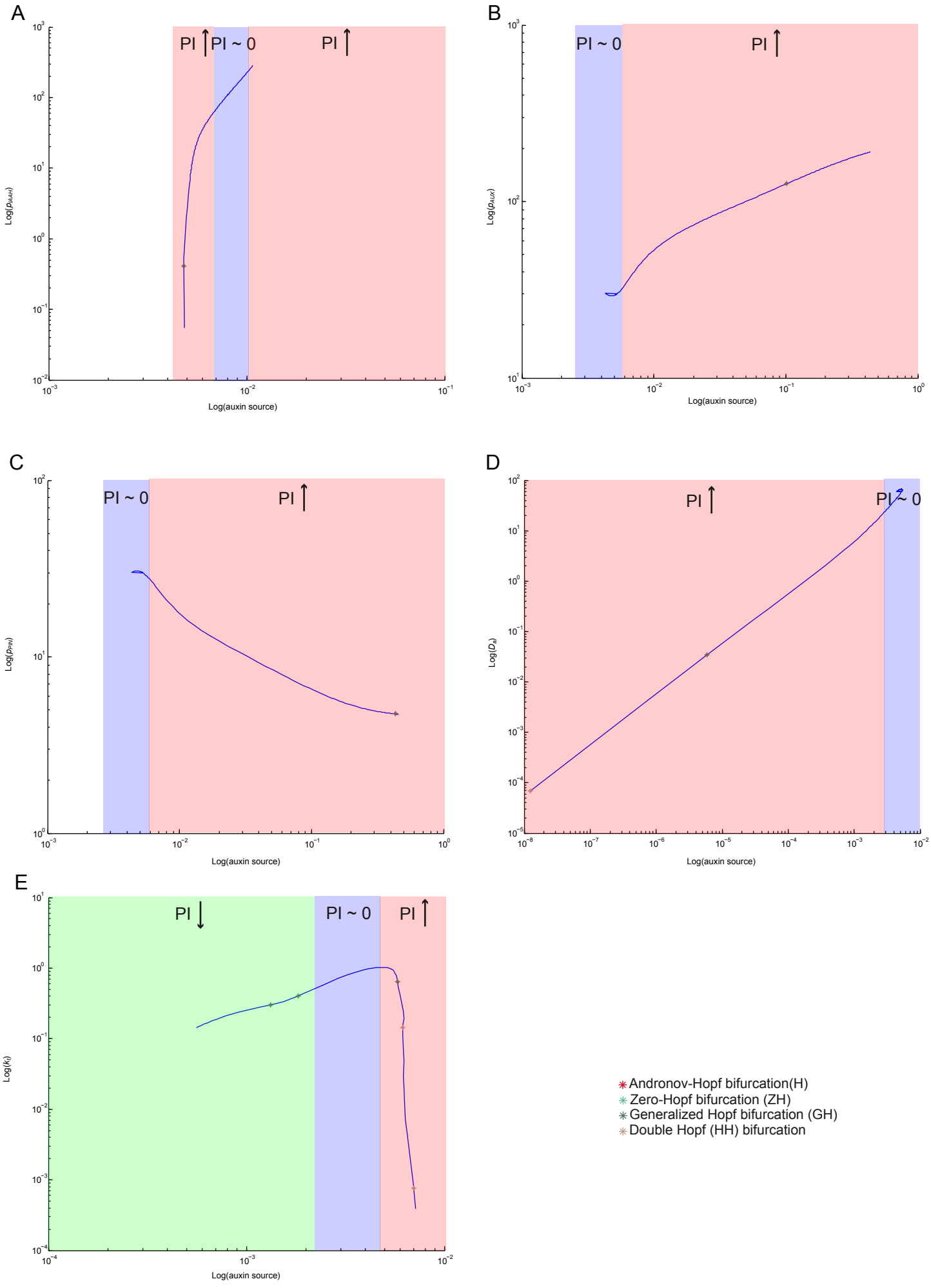
A
PI ↑
PI ~ 0
PI ↑
Log(p_{AUX})
Log(auxin source)
B
PI ~ 0
PI ↑
Log(p_{AUX})
Log(auxin source)
C
PI ~ 0
PI ↑
Log(p_{PIN})
Log(auxin source)
D
PI ↑
PI ~ 0
Log(D_a)
Log(auxin source)
E
PI ↓
PI ~ 0
PI ↑
Log(k_l)
Log(auxin source)
Andronov-Hopf bifurcation(H)
Zero-Hopf bifurcation (ZH)
Generalized Hopf bifurcation (GH)
Double Hopf (HH) bifurcation

Supplementary Figure 14. Two-dimensional bifurcation diagrams for equilibrium curves (1-5) presented in Supplementary Figure 13.

Analysis of model sensitivity and model behaviors associated with Polarization index (PI) are presented for the subsequent variation in strength of auxin source and one additional parameter: **(A)** passive auxin influx into cell (p_{IAAH}), **(B)** efficiency of AUX/LAX- dependent transport (p_{AUX}), **(C)** efficiency of PIN-dependent transport (p_{PIN}), **(D)** auxin diffusion in the cell wall (D_a), **(E)** saturation of polar auxin transport (k_t).

Polarization Index (PI) is described in Figure 2. The sign of PI corresponds to different model behavior (Supplementary Figure 13).

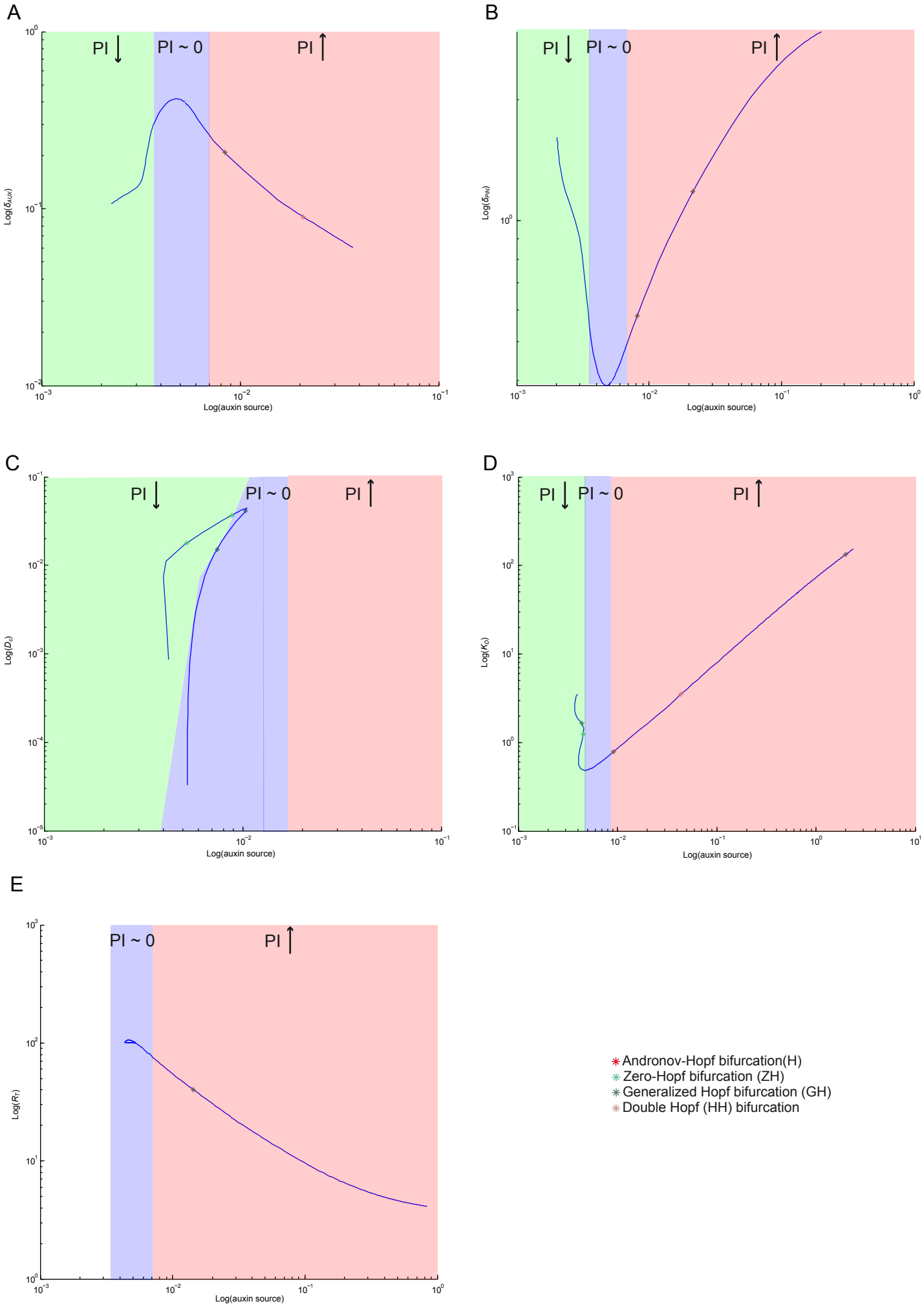
A
PI ↓
PI ~ 0
PI ↑
Log(δ_AUX)
Log(auxin source)
B
PI ↓
PI ~ 0
PI ↑
Log(δ_PIN)
Log(auxin source)
C
PI ↓
PI ~ 0
PI ↑
Log(D_A)
Log(auxin source)
D
PI ↓
PI ~ 0
PI ↑
Log(K_D)
Log(auxin source)
E
PI ~ 0
PI ↑
Log(R_T)
Log(auxin source)
Andronov-Hopf bifurcation(H)
Zero-Hopf bifurcation (ZH)
Generalized Hopf bifurcation (GH)
Double Hopf (HH) bifurcation

Supplementary Figure 15. Two-dimensional bifurcation diagrams for equilibrium curves (6-10) presented in Supplementary Figure 13.

Analysis of model sensitivity and model behaviors associated with Polarization index (PI) are presented for the subsequent variation in strength of auxin source and one additional parameter: **(A)** degradation of auxin influx carriers (δ_{AUX}), **(B)** degradation of auxin efflux carriers (δ_{PIN}), **(C)** diffusion of auxin-bound receptors in the cell wall (D_c), **(D)** receptor dissociation constant (K_D), **(E)** Amount of extracellular auxin receptors in the intercellular pools (R_T).

Polarization Index (PI) is described in Figure 2. The sign of PI corresponds to different model behavior (Supplementary Figure 13).

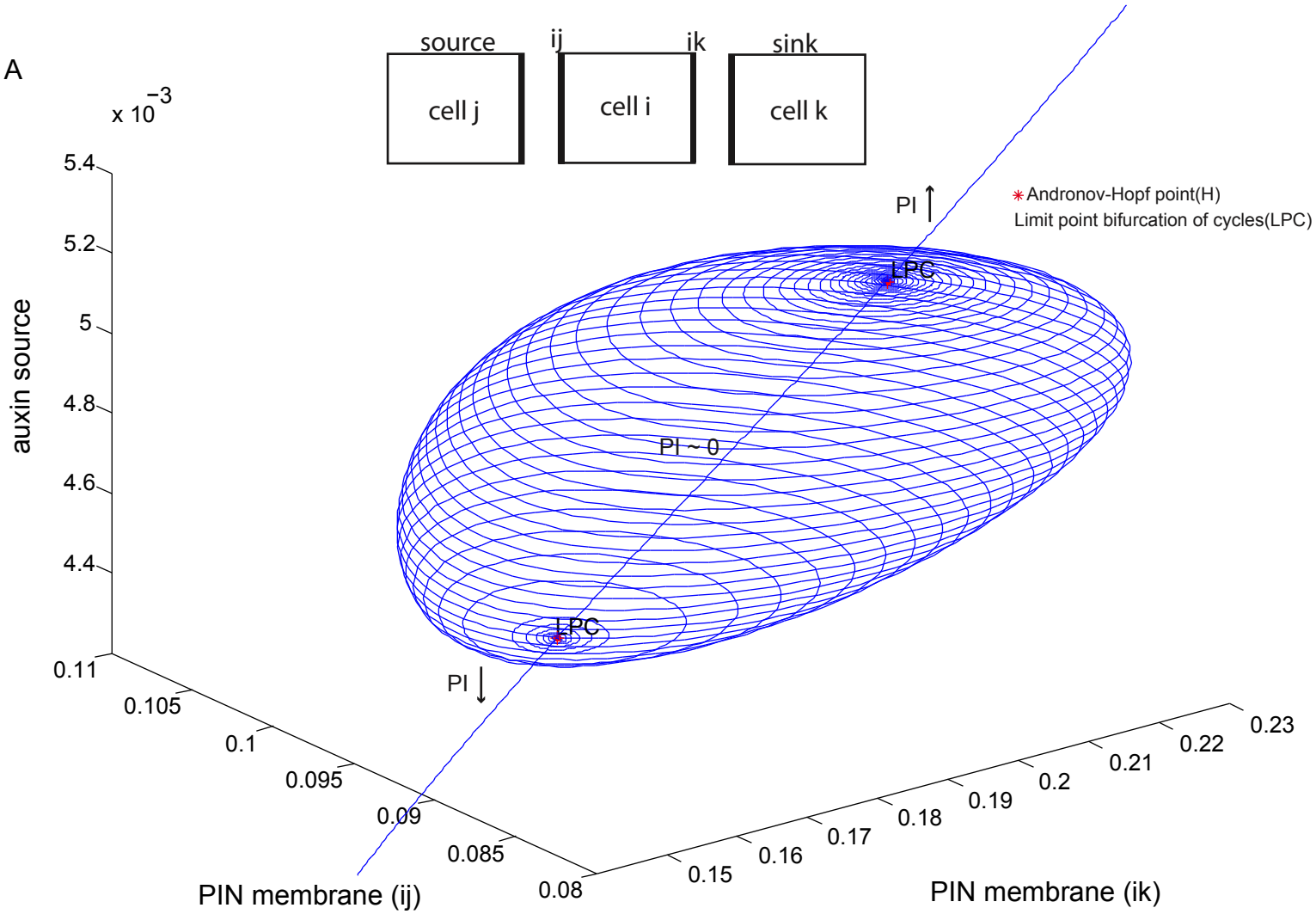
A
source
ij
ik
sink
cell j
cell i
cell k
x 10^-3
5.4
5.2
5
4.8
4.6
4.4
auxin source
Andronov-Hopf point(H)
Limit point bifurcation of cycles(LPC)
PI
LPC
PI ~ 0
LPC
PI
0.11
0.105
0.1
0.095
0.09
0.085
0.08
PIN membrane (ij)
0.23
0.22
0.21
0.2
0.19
0.18
0.17
0.16
0.15
PIN membrane (ik)

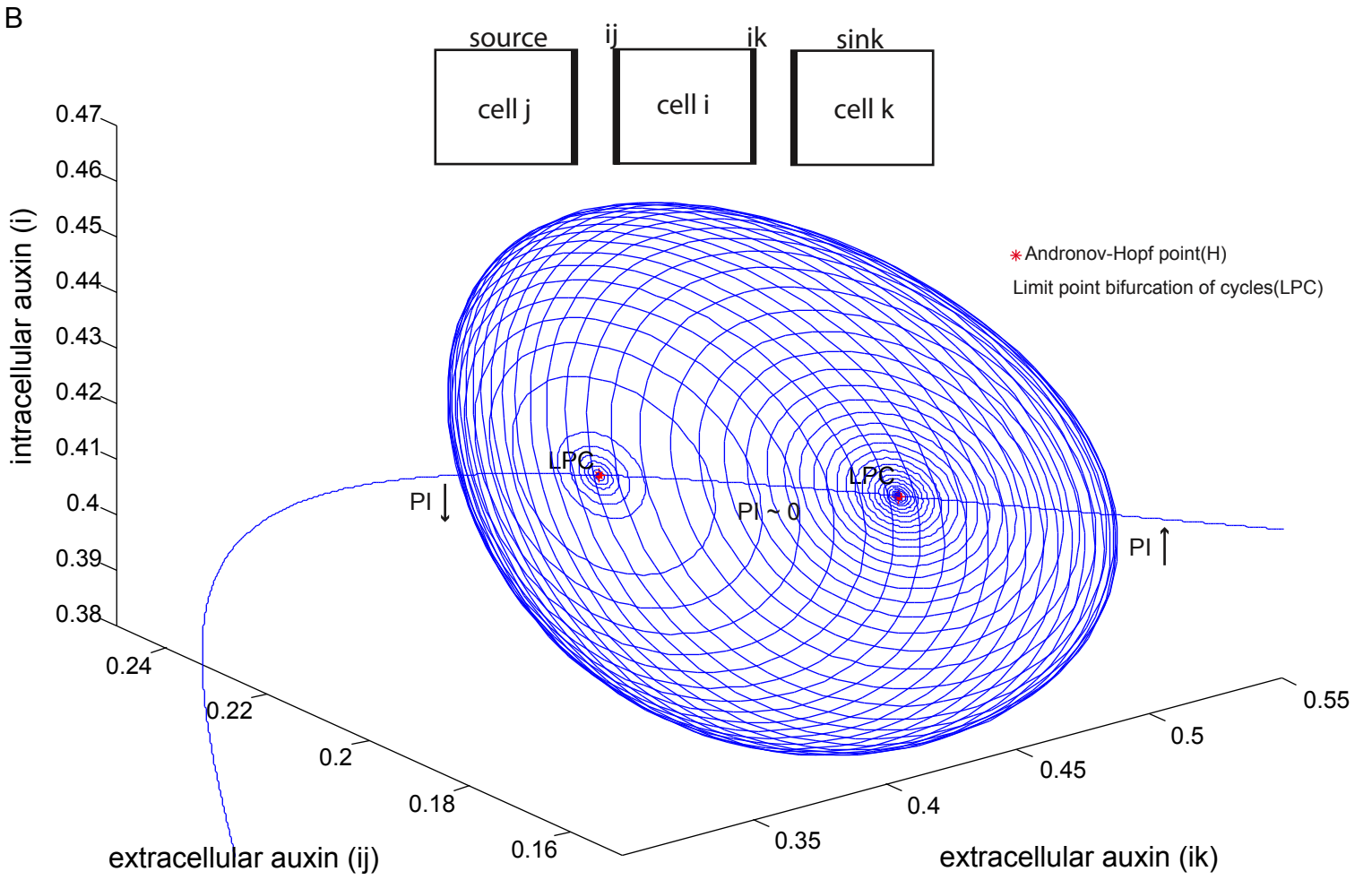
B
source
ij
ik
sink
cell j
cell i
cell k
0.47
0.46
0.45
0.44
0.43
0.42
0.41
0.4
0.39
0.38
intracellular auxin (i)
Andronov-Hopf point(H)
Limit point bifurcation of cycles(LPC)
LPC
LPC
PI
PI ~ 0
PI
0.24
0.22
0.2
0.18
0.16
extracellular auxin (ij)
0.55
0.5
0.45
0.4
0.35
extracellular auxin (ik)

Supplementary Figure 16. The periodic orbits of PIN and auxin levels correspond to stable limit cycle emerging from Hopf bifurcation.

(A) Stable limit cycle (LPC) connects two Hopf points (H). The variation of auxin source strength yielded the appearance of either oscillatory (PI ~ 0) or stable PIN polarization in the model (PI <> 0). **(B)** Phase portrait showing the borders between either oscillating (PI ~ 0) or stable (PI <> 0) auxin levels, inside and outside of the cell.

Polarization Index (PI) is described in Figure 2. The sign of PI corresponds to different model behavior (Supplementary Figure 13).

Model description

Auxin transport

According to the classical chemiosmotic hypothesis proposed by Raven [1] and Goldsmith [2], in the presence of high cytoplasmic pH (7.2-7.6), auxin is almost completely de-protonated and requires polar transport mediated by PINs to move across the plasma membrane (with permeability p_{PIN}) and consequently to leave the cell. In the apoplast at acidic pH (5.5), fractions of protonated and ionic auxin can either enter the cell via passive diffusion (with permeability p_{IAAH}) and is enhanced by the activity of influx carriers (AUX/LAX) (with permeability p_{AUX}). The model explicitly includes the movement of auxin within the apoplast [3] determined by diffusion coefficient D_a. The auxin movement between cells and within cell wall is given by:

$$\frac{dIAA_i}{dt} = \frac{1}{V_i}\cdot\left[p_{IAAH}\cdot\sum_{j\in N_i} l_{ij}\cdot(f_{in}^{+}(IAA_{ij}) - f_{out}^{+}(IAA_i))\right]$$

$$+\quad \frac{1}{V_i}\cdot\left[p_{PIN}\cdot\sum_{j\in N_i} PIN_{ij}\cdot(f_{in}^{-}(IAA_{ij}) - f_{out}^{-}(IAA_i))\right] \qquad (1)$$

$$+\quad \frac{1}{V_i}\cdot\left[p_{AUX}\cdot\sum_{j\in N_i} AUX_{ij}\cdot(f_{out}^{-}(IAA_{ij}) - f_{in}^{-}(IAA_i))\right]$$

$$\frac{dIAA_{ij}}{dt} = \frac{1}{V_{ij}}\cdot\left[D_a\cdot\left\{\frac{a_{ijji}}{d_{ijji}}\cdot(IAA_{ji} - IAA_{ij}) + \frac{a_{ijik}}{d_{ijik}}\cdot(IAA_{ik} - IAA_{ij}) + \frac{a_{ijil}}{d_{ijil}}\cdot(IAA_{il} - IAA_{ij})\right\}\right]$$

$$+\quad \frac{1}{V_{ij}}\cdot\left[p_{IAAH}\cdot l_{ij}\cdot(f_{out}^{+}(IAA_i) - f_{in}^{+}(IAA_{ij}))\right]$$

$$+\quad \frac{1}{V_{ij}}\cdot\left[p_{PIN}\cdot PIN_{ij}\cdot(f_{out}^{-}(IAA_i) - f_{in}^{-}(IAA_{ij}))\right] \qquad (2)$$

$$+\quad \frac{1}{V_{ij}}\cdot\left[p_{AUX}\cdot AUX_{ij}\cdot(f_{in}^{-}(IAA_i) - f_{out}^{-}(IAA_{ij}))\right]$$

with

$$f_{in}^{+}(IAA_{ij}) = \frac{IAA_{ij}}{1+10^{pH_{wall}-pK}}, \quad f_{out}^{+}(IAA_i) = \frac{IAA_i}{1+10^{pH_{cell}-pK}},$$

$$f_{in}^{-}(IAA_{ij}) = \frac{\Phi_{\inf lux}}{1+10^{-pH_{wall}+pK}} \cdot \frac{IAA_{ij}}{k_t + IAA_{ij}}, \quad f_{in}^{-}(IAA_i) = \frac{\Phi_{\inf lux}}{1+10^{-pH_{cell}+pK}} \cdot \frac{IAA_i}{k_t + IAA_i}, \tag{3}$$

$$f_{out}^{-}(IAA_{ij}) = \frac{\Phi_{efflux}}{1+10^{-pH_{wall}+pK}} \cdot \frac{IAA_{ij}}{k_t + IAA_{ij}}, \quad f_{out}^{-}(IAA_i) = \frac{\Phi_{efflux}}{1+10^{-pH_{cell}+pK}} \cdot \frac{IAA_i}{k_t + IAA_i}$$

where IAA_i is the mean auxin concentration in the i-th cell and IAA_{ij}, IAA_{ji}, IAA_{ik}, IAA_{il}, are the mean auxin concentrations in adjacent wall compartments (Figure 1, main text), V_i and V_{ij} are the dimensions of the cell and wall compartment, respectively. N_i denotes the number of direct neighbors of cell i. The PIN_{ij} and AUX_{ij} variables determine the average level of PINs and AUX/LAXs carriers at the i-th plasma membrane facing cell j. The parameter k_t defines the saturation constant of polar auxin transport. The parameter D_a describes auxin diffusion between the neighboring wall compartments. p_{IAAH}, p_{PIN}, p_{AUX} are the membrane permeabilities for passive diffusion and carrier mediated transport, respectively. The pH differs between cytoplasm and extracellular space (pH_{cell}, pH_{wall}) leading to different auxin fractions inside/outside of the cell: $f_{in}^{+}(IAA_{ij})$, $f_{in}^{-}(IAA_{ij})$, $f_{in}^{-}(IAA_i)$, $f_{out}^{+}(IAA_i)$, $f_{out}^{-}(IAA_{ij})$, $f_{out}^{-}(IAA_i)$ (Figure 1 – main text). Each wall compartment (ij) is considered to have three neighbors, left and right neighbors (il, ik) connected to the same cell i and one neighbor (ji) "connected" to the neighboring cell j. The crossing area between neighboring cytoplasm and membrane/wall compartments (for passive transport) is denoted as l_{ij}, crossing areas between neighboring wall compartments is a_{ijji}, a_{ijik}, a_{ijil} and distances between neighboring wall compartments used in the diffusion terms are given by d_{ijji}, d_{ijik}, d_{ijil}. For simplicity we used the constant value of a = 0.25 μm corresponding to cell wall thickness of 500 nm. In addition, the model assumes that the active auxin transport mediated by PINs and AUX/LAXs proteins

depends on the electrochemical gradient between cytoplasm and the apoplast. The Φ_{influx} and Φ_{efflux} parameters (eq. 3) describe the membrane potential:

$$\Phi_{\inf lux} = \Phi_{efflux} \cdot e^{\frac{zVF}{RT}} = \frac{zVF}{RT} \cdot \frac{e^{\frac{zVF}{RT}}}{e^{\frac{zVF}{RT}} - 1}, \quad (4)$$

where $V = -100\ mV$, $F = 9.6 \times 10^4\ mol^{-1}$, $R = 8.3\ Jmol^{-1}K^{-1}$, $T = 300K$.

Auxin carrier production and breakdown

We model the expression of AUX/LAX and PIN proteins in the cell as follows:

$$\frac{dPIN_i}{dt} = \alpha_{PIN} \cdot h(IAA_i) - \delta_{PIN} \cdot PIN_i \quad (5)$$

$$\frac{dAUX_i}{dt} = \alpha_{AUX} \cdot h(IAA_i) - \delta_{AUX} \cdot AUX_i \quad (6)$$

$$h(IAA_i) = \frac{IAA_i}{k_m + IAA_i} \quad (7)$$

where PIN_i and AUX_i are the total intracellular concentrations of PIN and AUX/LAX in cell i, α_{PIN} and α_{AUX} define the rates of auxin-induced PIN and AUX/LAX synthesis [4]-[6] and δ_{PIN} and δ_{AUX} determine decay rates of PIN and AUX/LAX proteins. IAA_i expresses the mean auxin concentration in the i-th cell and k_m is a Michaelis–Menten constant for auxin-dependent carrier production ($h(IAA_i)$, Figure 1B - main text).

Auxin carrier recycling

Auxin carriers recycle between endosomes and plasma membrane [7],[8] with the base rates a_{exo}, k_{exo} and a_{endo}, k_{endo} for AUX/LAX and PIN exocytosis (trafficking from endosomes to the plasma membrane) and their internalization (trafficking from plasma membrane to the endosomes), respectively. AUX/LAX transporters are distributed evenly on the cell membrane and show non-polar subcellular localization.

The AUX/LAX carriers are allocated in the plasma membrane in each time step as follows:

$$\frac{dAUX_{ij}}{dt} = a_{exo} \cdot AUX_i - a_{endo} \cdot AUX_{ij} \quad (8)$$

where AUX_{ij} represents the average amount of AUX/LAX proteins at the plasma membrane, and AUX_i is a total intracellular level of AUX/LAX in cell *i* and a_{exo} and a_{endo} are the rates of AUX/LAX exocytosis and internalization, respectively.

The corresponding change in intracellular AUX/LAX levels in *ith* cell is described as follows:

$$\frac{dAUX_i}{dt} = \sum_{j \in N_i} (a_{endo} \cdot AUX_{ij} - a_{exo} \cdot AUX_i) \quad (9)$$

The polar, subcellular localization of PIN auxin efflux facilitators in the model is determined by differential PIN retention at a given cell side [9] as a result of an auxin-dependent inhibition of PIN internalization [10] and an intracellular competition of cell membranes for auxin efflux transporters (Figure 1C, main text).

PIN allocation in the plasma membrane changes according to the following formula:

$$\frac{dPIN_{ij}}{dt} = k_{exo} \cdot PIN_i - PIN_{ij} \cdot (k_{endo} + kh_{ij}) \quad (10)$$

where PIN_{ij} are the PIN level on *ij*-th plasma membrane, and PIN_i is the total intracellular PIN level in *i*-th cell. The parameter k_{exo} determines the rate of PIN exocytosis, and k_{endo} is a base rate for PIN endocytosis whereas kh_{ij} determines the auxin-dependent effect on PIN internalization.

The corresponding change in intracellular PIN level in *ith* cell is given by:

$$\frac{dPIN_i}{dt} = \sum_{j \in N_i} (PIN_{ij} \cdot (k_{endo} + kh_{ij}) - k_{exo} \cdot PIN_i) \quad (11)$$

Auxin effect on PIN internalization

We assumed in our model that two neighboring cells share the intercellular pool of auxin receptors which we denote as $2R_T$. These extracellular receptors bind to auxin to form an active auxin-receptor complex (recruited receptor) whereas remaining free receptors from intercellular pool freely diffuse from one side of the cell to the closest side of adjacent cell. Because the amount of auxin receptors remains is conserved in the extracellular space between two neighboring cells, the mass conservation law is written as:

$$2R_T = R_{ij} + R_{ji} + C_{ij} + C_{ji} \tag{12}$$

where R_{ij} and R_{ji} are unbound/free solution receptors in the adjacent wall compartments, respectively and C_{ij} and C_{ji} are the active auxin-receptor complexes. The kinetics of the reversible auxin-receptor binding is given by:

$$IAA_{ij} + R_{ij} \xleftrightarrow{k_f, k_r} C_{ij}, \quad IAA_{ji} + R_{ji} \xleftrightarrow{k_f, k_r} C_{ji} \tag{13}$$

where k_f and k_r are forward and backward rates of receptor cycling between active and inactive states, respectively. Then a dissociation constant of auxin-receptor complex (K_D) is determined as:

$$K_D = \frac{kr}{kf} \tag{14}$$

Next the relative changes in the amount of bound and unbound receptors are governed by following ODE system:

$$\frac{dC_{ij}}{dt} = IAA_{ij} \cdot R_{ij} - K_D \cdot C_{ij} + D_c \cdot (C_{ji} - C_{ij}) \tag{15}$$

$$\frac{dC_{ji}}{dt} = IAA_{ji} \cdot R_{ji} - K_D \cdot C_{ji} - D_c \cdot (C_{ji} - C_{ij}) \tag{16}$$

$$\frac{dR_{ij}}{dt} = -IAA_{ij} \cdot R_{ij} + K_D \cdot C_{ij} + D_R \cdot (R_{ji} - R_{ij}) \tag{17}$$

$$\frac{dR_{ji}}{dt} = -IAA_{ji} \cdot R_{ji} + K_D \cdot C_{ji} - D_R \cdot (R_{ji} - R_{ij}) \tag{18}$$

where D_R is a free-receptor diffusion coefficient and D_C denotes the diffusion of the auxin-receptor complex. For simplicity we assume that auxin-receptor complexes and free receptors in *ij*-th and *ji*-th discrete wall compartments are practically in dynamic equilibrium (quasi-steady state) due to the fast kinetic reactions. In our model we considered the intercellular pools of extracellular receptor per each pair of neighboring cells such that the total amount of receptors in each intercellular pool is conserved. Therefore, the transversal diffusion of receptors can be negligible. To express that one puts the right side of equations (15)-(17) to zero whereas equation (18) can be replaced by equation (12). By solving the linear system of equations (12), (15)-(17) for *Cij*, $C_{ji,}$, R_{ij} and $R_{ji,}$ one obtains the following relations:

$$C_{ij} = \frac{2 \cdot R_T \cdot \left(\sqrt{\alpha \cdot \beta} \cdot (IAA_{ij} + IAA_{ji}) + IAA_{ij} \cdot (\alpha \cdot IAA_{ji} + K_D) \right)}{K_D \cdot (2 \cdot K_D + IAA_{ij} + IAA_{ji}) + 2 \cdot \sqrt{\alpha \cdot \beta} \cdot (IAA_{ij} + IAA_{ji} + 2 \cdot K_D) + \alpha \cdot (2 \cdot IAA_{ij} \cdot IAA_{ji} + IAA_{ij} \cdot K_D + IAA_{ji} \cdot K_D)} \tag{19}$$

$$C_{ji} = \frac{2 \cdot R_T \cdot \left(\sqrt{\alpha \cdot \beta} \cdot (IAA_{ij} + IAA_{ji}) + IAA_{ji} \cdot (\alpha \cdot IAA_{ij} + K_D) \right)}{K_D \cdot (2 \cdot K_D + IAA_{ij} + IAA_{ji}) + 2 \cdot \sqrt{\alpha \cdot \beta} \cdot (IAA_{ij} + IAA_{ji} + 2 \cdot K_D) + \alpha \cdot (2 \cdot IAA_{ij} \cdot IAA_{ji} + IAA_{ij} \cdot K_D + IAA_{ji} \cdot K_D)} \tag{20}$$

$$R_{ij} = \frac{2 \cdot R_T \cdot K_D (K_D + 2 \cdot \sqrt{\alpha \cdot \beta} + \alpha \cdot IAA_{ji})}{K_D \cdot (2 \cdot K_D + IAA_{ij} + IAA_{ji}) + 2 \cdot \sqrt{\alpha \cdot \beta} \cdot (IAA_{ij} + IAA_{ji} + 2 \cdot K_D) + \alpha \cdot (2 \cdot IAA_{ij} \cdot IAA_{ji} + IAA_{ij} \cdot K_D + IAA_{ji} \cdot K_D)} \tag{21}$$

$$R_{ji} = \frac{2 \cdot R_T \cdot K_D (K_D + 2 \cdot \sqrt{\alpha \cdot \beta} + \alpha \cdot IAA_{ji})}{K_D \cdot (2 \cdot K_D + IAA_{ij} + IAA_{ji}) + 2 \cdot \sqrt{\alpha \cdot \beta} \cdot (IAA_{ij} + IAA_{ji} + 2 \cdot K_D) + \alpha \cdot (2 \cdot IAA_{ij} \cdot IAA_{ji} + IAA_{ij} \cdot K_D + IAA_{ji} \cdot K_D)} \tag{22}$$

where $\alpha = \frac{D_C}{D_R}$, and $\beta = D_C \cdot D_R$.

We assumed that the active auxin-receptor complexes are recruited with the highest probability to the nearest cell. Because recruited receptors transfer a signal to the plasma membrane they could be temporally immobilized at the cell surface (represented by discrete wall compartment) presumably due to its interaction with plasma membrane or its conformational changes. Therefore, the diffusion of free receptor in the apoplast becomes much larger than the diffusion of auxin-bound recptors ($D_C << D_R$) which then implicates $\alpha \sim 0$ and $\beta \sim 0$ for finite values of D_R and, D_C. In this case of $D_C = 0$ and $D_R \to \infty$ the equations (19)-(22) simplify to:

$$C_{ij} = \frac{2 \cdot R_T \cdot IAA_{ij}}{(2 \cdot K_D + IAA_{ij} + IAA_{ji})} \tag{23}$$

$$C_{ji} = \frac{2 \cdot R_T \cdot IAA_{ji}}{(2 \cdot K_D + IAA_{ij} + IAA_{ji})} \tag{24}$$

$$R_{ij} = R_{ji} = \frac{2 \cdot R_T \cdot K_D}{(2 \cdot K_D + IAA_{ij} + IAA_{ji})} \tag{25}$$

In our model we assume that the recruited receptors signal on PIN internalization. Taking into account equations (23)-(25) one derives the formula that describes the auxin-dependent inhibition of PIN internalization at the *(ij)* side of the *i*-th cell:

$$kh_{ij} = \frac{\mu}{1 + C_{ij}} \tag{26}$$

where kh_{ij} expresses the effective rate of PIN endocytosis (μ) repressed by the amount of active signalling components at *ijth* side of the cell as presented in Figures 1D and 2A in the main text.

Tissue layout

Two representations of a longitudinal section of the shoot apical meristem, including a two-dimensional grid and a cellular template with irregular cell topology, were used to simulate auxin transport during auxin canalization, vein loop formation, and tissue wounding. Depending on the specific case simulated, a single cell is either a square (grid representation) or an arbitrary polygon (longitudinal meristem section). Each cell was surrounded by wall compartments that included plasma membranes and the apoplast (extracellular space). A cell volume of 100 μm^2 and a wall length of 10 μm in the two-dimensional were adopted in the grid tissue layout. The intracellular gradients in the grid tissue layout (Supplementary Figure 11) were modeled as follows:

The single cell box was divided in four identical triangular compartments each associated with the one side of the cell and the cell center. In this case, intracellular auxin freely diffuses within intracellular compartments following Fick's law:

$$J_{1->2} = -D \cdot \frac{c_1 - c_2}{L} \tag{27}$$

where $J_{1->2}$ is the net flux from compartment 1 to compartment 2, c_j is the concentration of intracellular auxin in compartment j for j=1,2, and D is the diffusion coefficient of auxin in the cell, and L is a distance between compartments.

In the cellular templates, the cell volume and cell wall length varied, but were, on average, approximately 98 μm^2 and 9 μm, respectively. For simplicity, cell wall thickness was set at 0.5 μm.

Boundary conditions

In the computer simulations of auxin canalization and tissue wounding (Figures 3, 4, and 7), the auxin source was represented by a cell that produced auxin at a rate of 0.0015 μM μm^{-2} s^{-1}. The auxin sink was placed at the bottom-most part of the tissue (grid and cellular

tissue layouts) and to the right-most cell in simulations on the file of cells and corresponded to the site of the tissue where auxin was evacuated from the system (sink preserves near zero auxin concentration). For the remaining tissue borders in all model simulations, zero-flux boundary conditions were used. Virtual wounding (Figure 7) was represented by cell ablation (simply by removing cells from the tissue layout). For the simulations of vein loop patterns (Figure 5), the primary source was as above (Figures 3 and 4), and the secondary auxin sources were sites of enhanced auxin production at the rate of 0.001 $\mu M\ \mu m^{-2}\ s^{-1}$ (each source). In competitive canalization simulations (Figure 6), the pea stem decapitation corresponded to a strong reduction of strength of the primary auxin source by 10-fold but not its complete removal which would result in the suppression of stable PIN polarization pattern (Supplementary Figure 12). Most of the auxin biosynthesis is indeed coming from the decapitated region, however also the vascular tissue is the site of local auxin biosynthesis. Therefore we reduced the auxin level, which is likely to reflect *in planta* situation. The weak and strong auxin sources were represented by auxin-producing cells at rates of 0.0002 $\mu M\ \mu m^{-2}\ s^{-1}$ and 0.002 $\mu M\ \mu m^{-2}\ s^{-1}$, respectively.

Cell expansion and cell division

Cellular growth was described by cell expansion and was regulated by auxin in a concentration-dependent manner [14] and subsequent cell division. The tissue dynamics encompassed threshold of cell size above which cells start to divide. The arbitrary division threshold was set at 1000 μm^2. For simplicity in the model, the pro-vascular cells undergo the auxin-dependent differentiation to mature cells. Once those cells reached maturity they lose their capability to divide [15]. We assumed that high auxin concentrations in the tissue promote vascular differentiation [15]. Simulations of growing tissue (Figure 4C-E) were carried out over 3 CPU time days, which corresponds to 259,200 simulation steps.

Numerical and simulation methods

The dynamic cell-based simulations of auxin transport were done by numerical computations of coupled ODE systems, with an adaptive-size, fifth-order Runge-Kutta method with monitoring of local truncation error to ensure accuracy and adjustment of the step size. A time step was adjusted in each iteration to minimize local calculation errors. If the local truncation error was small enough, the method gave the output for the defined time interval and then proceeded to the next time step. A time interval of 1 s was used, but other values were also tested without significant changes in the qualitative results of the simulations. For the sensitivity and bifurcation analysis of the stationary solutions (Supplementary Figures 13-16), we used MATCONT - graphical Matlab package for numerical bifurcation analysis [16].

Parameters

The general parameters for tissue layout and model simulations are shown in Supplementary Table 1. The parameters for auxin transport dynamics are presented in Supplementary Table 2, and were mainly derived from the literature [2], [3], [11]-[13]. The quantitative parameters for PIN and AUX/LAX recycling, production and degradation remain to a large extent unknown and were chosen to assert that auxin carriers recycling is a much faster process than an auxin carrier expression. They are presented in Supplementary Table 3.

Model sensitivity analysis

We analyzed the importance of each component of the ERP model for general model behavior, sensitivity and robustness. Our model analysis was divided in four parts; each part treats about one structural component of the ERP model. For instance, we investigated the altered dynamics of extracellular receptor-based auxin signalling mechanism by modifying diffusion rates of bound and unbound receptors, the amount of receptors in the intercellular pools and specificity of auxin binding (receptor recruitment) (Supplementary Figures 1-3). We

concluded that the competitive utilization of auxin receptors in the apoplast determined by their respective motility is the actual trigger for initiation of PIN polarization. Therefore, we found that auxin-mediated carrier expression plays a crucial role in generating realistic PIN polarization patterns during vascularization and tissue regeneration (Supplementary Figures 4 and 5). Also the *in silico* interference with the main components of polar auxin transport system that includes PIN and AUX/LAX transporters led to the surprising observations (Supplementary Figures 6 and 7). In particular, the contribution of AUX/LAX-dependent transport to PIN polarization maintenance has been revealed (Supplementary Figure 7). Also the general role of polar auxin transport in buffering auxin diffusion in the apoplast to maintain cell polarities has been suggested (Supplementary Figures 8 and 9). Then we tested the robustness of the ERP model with respect to the auxin source/sink translocation and presence of intracellular diffusion-driven auxin gradients (Supplementary Figures 10 and 11). We also found that auxin biosynthesis play a crucial role in stabilizing PIN polarization and polar auxin transport in the tissue (Supplementary Figure 12) and their spatio-temporal regulation may be linked to phenomena such as vascular attraction/repulsion and competitive canalization of auxin flow in shoot branching. To investigate model behavior, we analyzed the sensitivity and robustness of stationary solutions with respect to perturbations in model parameters (Supplementary Figures 13-16). We identified the parameter regimes for which our model exhibits particular type of behavior (Supplementary Figures 13-16).

Supplementary Tables

Supplementary Table 1. General parameters for tissue layout and model simulations

Parameter	Cell file	Grid layout	Cellular layout	Cellular growth	Units
Cell area (V_i)	100	100	98*	variable	μm^2
Wall area (V_{ij})	0.1 x V_i	0.1 x V_i	0.1 x V_i^*	variable	μm^2
Wall length (l_{ij})	10	10	9.8*	variable	µm
Wall thickness term (a_{ijji}/d_{ijji})	0.025	0.025	0.025	0.025	µm
Time step	1	1	1	1	s
Growth step	-	-	-	1	min
Cell expansion rate	-	-	-	0.01	-
Cell division threshold	-	-	-	1000	μm^2

* Mean cell and wall volumes and mean wall length for cellular tissue layout

Supplementary Table 2. Auxin transport parameters

Parameter	Fig. 2,3,4,5,6,7 and Supp Fig 2,4,5,10,12	Supp Fig 1	Supp Fig 3	Supp Fig 6	Supp Fig 7	Supp Fig 8	Supp Fig 9	Supp Fig 11	Units
Apoplastic diffusion (D_a)	100	100	100, 10	100	100	100, 10	500, 20	100	$\mu m^2 s^{-1}$
Free receptor diffusion (D_R)	1	1, 0.1, 10 , 100	1	1	1	1	1	1	$\mu m^2 s^{-1}$
Auxin-receptor complex diffusion (D_C)	0	0, 0.001, 0.1, 1	0	0	0	0	0	0	$\mu m^2 s^{-1}$
IAAH permeability (p_{IAAH})	10	10	10	10	100, 10	10	50, 10	10	$\mu m\, s^{-1}$
PIN permeability (p_{PIN})	30	30	30	300, 30, 1	30	30	150, 30	30	$\mu m\, s^{-1}$
AUX/LAX permeability (p_{AUX})	30	30	30	30	300, 30, 1	30	150, 30	30	$\mu m\, s^{-1}$
pH in wall (pH_{wall})	5.5	5.5	5.5	5.5	5.5	5.5	5.5	5.5	-
pH in cell (pH_{cell})	7.6	7.6	7.6	7.6	7.6	7.6	7.6	7.6	-
Dissociation constant (pK)	5	5	5	5	5	5	5	5	-
Saturation constant for auxin transport (k_t)	1	1	1	1	1	10, 1	1	1	µM
Intracellular auxin diffusion (D)	-	-	-	-	-	-	-	600, 300, 100, 50, 10	$\mu m^2 s^{-1}$

Supplementary Table 3. PIN and AUX/LAX dynamics

Parameter	Fig.2,3,4,5,6,7 and Supp Fig 1,6,7,8,9,10,11,12	Supp Fig 2	Supp Fig 3	Supp Fig 4, 5	Units
PIN exocytosis base rate (k_{exo})	1	1	1	1	s^{-1}
PIN internalization base rate (k_{endo})	0.001	0.001	0.001	0.001	s^{-1}
Effective PIN internalization (μ)	1	1, 0.1	1	1	s^{-1}
AUX/LAX exocytosis base rate (a_{exo})	1	1	1	1	s^{-1}
AUX/LAX internalization base rate (a_{endo})	0.1	0.1	0.1	0.1	s^{-1}
PIN production rate (α_{PIN})	1	1	1	1, 0.1, 0.01, 0	s^{-1}
PIN degradation rate (δ_{PIN})	0.03	0.03	0.03	0.03, 0.001, 0	s^{-1}
AUX/LAX production rate (α_{AUX})	1	1	1	1, 0.1, 0.01, 0	s^{-1}
AUX/LAX degradation rate (δ_{AUX})	0.05	0.05	0.05	0.05, 0.001, 0	s^{-1}
Saturation of auxin-induced PIN and AUX/LAX production (k_m)	100	100	100	100	μM
Receptor dissociation constant (K_D)	1	1	10, 1, 0.1	1	μM
The number of extracellular auxin receptors (R_T)	100	10000, 100, 1	100	100	-

Supplementary Movies

Supplementary Movie 1

The file contains Supplementary Movie 1 displaying the PIN-dependent auxin canalization on grid layout (simulation of Fig. 3A-C). Color coding schemes for auxin concentrations and PIN levels that were used in the model simulations as described in Fig. 3I. Auxin concentrations can vary from 0 (black) to 10 (bright green). PIN levels at the plasma membrane may change from 0 (black) to 10 (bright red). White arrows point in the direction of the preferential PIN polarity, and arrow size indicates the relative strength of PIN expression in the cell.

Supplementary Movie 2

The file contains Supplementary Movie 2 showing the PIN-dependent auxin canalization on cellular layout (simulation of Fig. 3D, G, H). Color coding schemes for auxin concentrations and PIN levels that were used in the model simulations as described in Fig. 3I. Auxin concentrations can vary from 0 (black) to 10 (bright green). PIN levels at the plasma membrane may change from 0 (black) to 10 (bright red). White arrows point in the direction of the preferential PIN polarity, and arrow size indicates the relative strength of PIN expression in the cell.

Supplementary Movie 3

The file contains Supplementary Movie 3 showing PIN polarity and auxin distribution associated with auxin canalization during dynamic cellular growth over 3 CPU days (simulation of Fig. 4C-E). Color coding schemes for auxin concentrations and PIN levels that were used in the model simulations as described in Fig. 3I. Auxin concentrations can vary

from 0 (black) to 10 (bright green). PIN levels at the plasma membrane may change from 0 (black) to 10 (bright red). White arrows point in the direction of the preferential PIN polarity, and arrow size indicates the relative strength of PIN expression in the cell.

Supplementary Movie 4

The file contains Supplementary Movie 4 displaying the formation of vein loop pattern (simulation of Fig. 5C-H). Auxin concentrations can vary from 0 (black) to 10 (bright green). PIN levels at the plasma membrane may change from 0 (black) to 10 (bright red). White arrows point in the direction of the preferential PIN polarity, and arrow size indicates the relative strength of PIN expression in the cell.

Supplementary Movie 5

The file contains Supplementary Movie 5 addressing competitive canalization and lateral bud release (simulation of Fig. 6A-E). Auxin concentrations can vary from 0 (black) to 10 (bright green). PIN levels at the plasma membrane may change from 0 (black) to 10 (bright red). White arrows point in the direction of the preferential PIN polarity, and arrow size indicates the relative strength of PIN expression in the cell.

Supplementary Movie 6

The file contains Supplementary Movie 6 showing competitive canalization and apical dominance (simulation of Fig. 6I-M). Auxin concentrations can vary from 0 (black) to 10 (bright green). PIN levels at the plasma membrane may change from 0 (black) to 10 (bright red). White arrows point in the direction of the preferential PIN polarity, and arrow size indicates the relative strength of PIN expression in the cell.

Supplementary Movie 7

The file contains Supplementary Movie 7 illustrating the vascular tissue regeneration after wounding (simulation of Fig. 7). Color coding schemes for auxin concentrations and PIN levels that were used in the model simulations as described in Fig. 3I. Auxin concentrations can vary from 0 (black) to 10 (bright green). PIN levels at the plasma membrane may change from 0 (black) to 10 (bright red). White arrows point in the direction of the preferential PIN polarity, and arrow size indicates the relative strength of PIN expression in the cell.

Additional references

1. Raven JA (1975) Transport of Indoleacetic-Acid in Plant-Cells in Relation to Ph and Electrical Potential Gradients, and Its Significance for Polar Iaa Transport. *New Phytologist* **74**: 163-172.
2. Goldsmith, M. H. M., Goldsmith, T. H. & Martin, M. H. Mathematical analysis of the chemosmotic polar diffusion of auxin through plant tissues. *PNAS.* **78**: 976-980 (1981).
3. Mitchison, G.J. The dynamics of auxin transport. *Proceedings of the Royal Society B: Biological Sciences* **209**: 489-511 (1980a).
4. Heisler, M. G. *et al.* Patterns of auxin transport and gene expression during primordium development revealed by live imaging of the *Arabidopsis* inflorescence meristem. *Curr. Biol.* **15**: 1899-1911 (2005).
5. Scarpella, E., Marcos, D., Friml, J. & Berleth, T. Control of leaf vascular patterning by polar auxin transport. *Genes Dev.* **20**: 1015-1027 (2006).
6. Vieten A., Vanneste S., Wisniewska J., Benkova E., Benjamins R., Beeckman T., Luschnig C., Friml J. Functional redundancy of PIN proteins is accompanied by auxin-dependent cross-regulation of PIN expression. *Development* **132**: 4521-4531 (2005).
7. Geldner, N., Xu, J., Uemura, T., Chory, J., Ueda, T., Nakano, A., Scheres, B. and Friml, J. Generation of cell polarity in plants links endocytosis, auxin distribution and cell fate decisions.. *Nature* **456**: 962-966 (2008).
8. Steinmann T, Geldner N, Grebe M, Mangold S, Jackson CL, et al. (1999) Coordinated polar localization of auxin efflux carrier PIN1 by GNOM ARF GEF. *Science* **286**: 316-318.
9. Dhonukshe, P., Tanaka, H., Goh, T., Ebine, K., Mähönen, AP., Prasad, K., Blilou, I., Geldner, N., Xu, J., Uemura, T., Chory, J., Ueda, T., Nakano, A., Scheres, B. and Friml, J. Generation of cell polarity in plants links endocytosis, auxin distribution and cell fate decisions. *Nature*

456: 962-966 (2008).

10. Paciorek, T., Zazimalová, E., Ruthard, N., Petrasek, J., Stierhof, J.D., Kleine-Vehn, J., Morris, D.A., Emans, N., Jurgens, G., Geldner, N., Friml, J. Auxin inhibits endocytosis and promotes its own efflux from cells. *Nature* **435**: 1251-1256 (2005).

11. Kramer, E.M. How far can a molecule of weak acid travel in the apoplast or xylem? *Plant Physiology* **141:** 1233-1236 (2006).

12. Swarup, R *et al*. Root gravitropism requires lateral root cap and epidermal cells for transport and response to a mobile auxin signal. *Nature Cell Biol*. **7**: 1057-1065 (2005).

13. Kramer, E. M., Frazer, N. L. and Baskin, T. I. Measurement of diffusion within the cell wall in living roots of *Arabidopsis thaliana J. Exp. Bot.* **58:** 3005-3015 (2007).

14. Chen J-G, Ullah H, Young JC, Sussman MR, Jones AM (2001) ABP1 is required for organized cell elongation and division in *Arabidopsis* embryogenesis. *Genes Dev* **15**: 902-911.

15. Ye Z-H (2002) Vascular tissue differentiation and pattern formation in plants. *Annu Rev Plant Biol* **53**: 183-202.

16. Dhooge A., Govaerts W. and Kuznetsov Yu.A. (2003) MatCont: A MATLAB package for numerical bifurcation analysis of ODEs. *ACM TOMS* **29**:141-164.

17. Tromas, A., et al. (2010) AUXIN BINDING PROTEIN 1: functional and evolutionary aspects. *Trends Plant Sci* **15**: 436-446.

Pseudo c++ source code for the ERP model

```
/*
 *  The Virtual Leaf is free software: you can redistribute it and/or
modify
 *  it under the terms of the GNU General Public License as published by
 *  the Free Software Foundation, either version 3 of the License, or
 *  (at your option) any later version.
 *
 *  The Virtual Leaf is distributed in the hope that it will be useful,
 *  but WITHOUT ANY WARRANTY; without even the implied warranty of
 *  MERCHANTABILITY or FITNESS FOR A PARTICULAR PURPOSE.  See the
 *  GNU General Public License for more details.
 *
 *  You should have received a copy of the GNU General Public License
 *  along with the Virtual Leaf.  If not, see
<http://www.gnu.org/licenses/>.
 *
*/
// Pseudo code (C++) for the ERP model definition in Virtual Leaf
framework
//-------------------------------------------------//
// Defines maximum number of chemicals in the model
//const int Cell::nchem = 5;

// class Parameter is a container for all model parameters (Virtual Leaf
framework)
// Parameter *par;

// class Wall defines wall interface implementation in Virtual Leaf
framework
// Wall *w;

// class Cell defines cell interface implementation in Virtual Leaf
framework
// Cell *c;

// w->C1() and w->C2() are wall object functions that return neighboring
cell objects (C1, C2)

// c->Chemical(i) gives i-th chemical in the cell

// w->Apoplast(i) gives i-th chemical in the wall

// w->Transporter1(i) gives i-th auxin transporter on the cell membrane
of Cell C1

// w->Transporter2(i) gives i-th auxin transporter on the cell membrane
of Cell C2

// Copyright 2010 Krzysztof Wabnik
//  krwab@psb.vib-ugent.be
```

```
//-------------------------------------------------//

 // Fractions of auxin

    double f_AH_cell = 1 / (1 + pow(10,(par->pH_cyto - par->pK)));
      double f_AH_wall = 1 / (1 + pow (10, (par->pH_wall -par->pK)));
      double f_A_cell= 1 / (1 + pow(10,(-par->pH_cyto + par->pK)));
      double f_A_wall= 1 / (1 + pow (10, (-par->pH_wall +par->pK)));

// Interface class for auxin transport
class AuxinTransport : public TransportFunction {

 public:
  virtual void operator()(Wall *w, double *dchem_c1, double *dchem_c2,
double *dap) {







// passive auxin diffusion: cell interface -> wall interface (cells C1
and C2 are neighbors)

   // Cell C1
     dchem_c1[0] += par->piaah * (w->Length() / w->C1()->Area()) *
(f_AH_wall * w->Apoplast(0) - f_AH_cell * w->C1()->Chemical(0));

       // Cell C2
     dchem_c2[0] += par->piaah * (w->Length() / w->C2()->Area()) *
(f_AH_wall * w->Apoplast(1) - f_AH_cell * w->C2()->Chemical(0));

// passive auxin diffusion: wall interface -> cell interface

  // Wall compartment 1
      dap[0] += par->piaah * (w->Length() / w->Area()) * (f_AH_cell * w-
>C1()->Chemical(0) - f_AH_wall * w->Apoplast(0));

      // Wall compartment 2
      dap[1] += par->piaah * (w->Length() / w->Area()) * (f_AH_cell * w-
>C2()->Chemical(0) - f_AH_wall * w->Apoplast(1));




// Auxin diffusion in the apoplast

   dap[0] += par->Da * (par->aijji / par->dijji)*(1 / w->Area()) * (w-
>Apoplast(1) - w->Apoplast(0));
   dap[1] += par->Da * (par->aijji / par->dijji)*(1 / w->Area()) *(w-
>Apoplast(0) - w->Apoplast(1));
```

```
// Transversal auxin diffusion in the apoplast
   int ind1=0.;
   int ind2=0.;
   double trans_c1= w->C1()->GiveTrans(w, ind1); // total auxin influx
from neighboring wall compartments surrounding cell C1
   double trans_c2= w->C2()->GiveTrans(w, ind2);// total auxin influx
from neighboring wall compartments surrounding cell C2

   dap[0] += par->Da * (par->aijji / par->dijji) * (1 / w->Area()) *
(trans_c1 - ind1 * w->Apoplast(0));
   dap[1] += par->Da * (par->aijji / par->dijji) * (1 / w->Area()) *
(trans_c2 - ind2 * w->Apoplast(1));

// Active auxin transport: cell interface -> wall interface (PINs)

   // Cell C1
   dchem_c1[0]-= par->p_pin * (1 / w->C1()->Area())  * (f_A_cell * par-
>Nefflux * w->Transporters1(0) * w->C1()->Chemical(0) / (par->kt + w-
>C1()->Chemical(0)));
   dchem_c1[0]+= par->p_pin * (1 / w->C1()->Area()) * (f_A_wall * par-
>Ninflux * w->Transporters1(0) * w->Apoplast(0) / (par->kt + w-
>Apoplast(0)));

   // Cell C2
   dchem_c2[0]-= par->p_pin  * (1 / w->C2()->Area()) * (f_A_cell * par-
>Nefflux * w->Transporters2(0) * w->C2()->Chemical(0) / (par->kt + w-
>C2()->Chemical(0)));

   dchem_c2[0]+= par->p_pin  * (1 / w->C2()->Area()) * (f_A_wall * par-
>Ninflux * w->Transporters2(0) * w->Apoplast(1) / (par->kt + w-
>Apoplast(1)));
// Active auxin transport: wall interface -> cell interface (PINs)
   dap[0] += par->p_pin  * (1 / w->Area()) * (f_A_cell * par->Nefflux *
w->Transporters1(0) * w->C1()->Chemical(0) /(par->kt + w->C1()-
>Chemical(0)));
   dap[0] -= par->p_pin  * (1/w->Area()) * (f_A_wall * par->Ninflux * w-
>Transporters1(0) * w->Apoplast(0)/ (par->kt + w->Apoplast(0)));
   dap[1] += par->p_pin  * (1/w->Area()) * (f_A_cell * par->Nefflux * w-
>Transporters2(0) * w->C2()->Chemical(0) /(par->kt + w->C2()-
>Chemical(0)));
   dap[1] -= par->p_pin  * (1/w->Area()) * (f_A_wall * par->Ninflux * w-
>Transporters2(0) * w->Apoplast(1)/ (par->kt + w->Apoplast(1)));

// Active auxin transport: cell interface -> wall interface (AUX\LAXs)

    // Cell C1
     dchem_c1[0]+= par->p_aux * (1 / w->C1()->Area()) * (f_A_wall * par-
>Nefflux * w->Transporters1(1) * w->Apoplast(0) / (par->kt + w-
>Apoplast(0)));
     dchem_c1[0]-= par->p_aux * (1 / w->C1()->Area()) * (f_A_cell * par-
>Ninflux * w->Transporters1(1) * w->C1()->Chemical(0) / (par->kt + w-
>C1()->Chemical(0)));
```

```
      // Cell C2
      dchem_c2[0]+= par->p_aux * (1 / w->C2()->Area()) *(f_A_wall * par-
>Nefflux * w->Transporters2(1) * w->Apoplast(1) / (par->kt + w-
>Apoplast(1)));
      dchem_c2[0]-= par->p_aux * (1 / w->C2()->Area()) * (f_A_cell * par-
>Ninflux * w->Transporters2(1) * w->C2()->Chemical(0) / (par->kt + w-
>C2()->Chemical(0)));

// Active auxin transport: wall interface -> cell interface (AUX\LAXs)

   dap[0] -= par->p_aux  * (1 / w->Area()) * (f_A_wall * par->Nefflux *
w->Transporters1(1) * w->Apoplast(0) / (par->kt + w->Apoplast(0)));
   dap[0] += par->p_aux  * (1 / w->Area()) * (f_A_cell * par->Ninflux *
w->Transporters1(1) * w->C1()->Chemical(0) / (par->kt + w->C1()-
>Chemical(0)));
   dap[1] -= par->p_aux  * (1 / w->Area()) * (f_A_wall * par->Nefflux *
w->Transporters2(1) * w->Apoplast(1) / (par->kt + w->Apoplast(1)));
   dap[1] += par->p_aux  * (1 / w->Area()) * (f_A_cell * par->Ninflux *
w->Transporters2(1) * w->C2()->Chemical(0) / (par->kt + w->C2()-
>Chemical(0)));


// Source and Sink definition

// Sources an Sinks

       if (w->C2()->Boundary() == Cell::SOURCE) { // Cell C1 is source
        double aux_flux = par->auxin_source * w->Length() ;
                 dchem_c2[0] += aux_flux;
            }

         if (w->C1()->Boundary() == Cell::SOURCE) { // Cell C2 is source
        double aux_flux = par->auxin_source * w->Length() ;
                 dchem_c1[0] += aux_flux;

            }

         if (w->C2()->Boundary() == Cell::SINK) { // Cell C1 is sink
            dchem_c2[0] -= par->auxin_sink * w->C2()->Chemical(0);

            }

         if (w->C1()->Boundary() == Cell::SINK) { // Cell C2 is sink
            dchem_c1[0] -= par->auxin_sink * w->C1()->Chemical(0);

            }

// Ablated Cells

      if (w->C1()->Boundary() == Cell::DEAD){

            dchem_c1[0] -= w->C1()->Chemical(0);
                 dchem_c1[1] -= w->C1()->Chemical(1);
```

```
      }

      if (w->C2()->Boundary() == Cell::DEAD){

            dchem_c2[0] -= w->C2()->Chemical(0);
                  dchem_c2[1] -= w->C2()->Chemical(1);


      }

};
};


// Interface class for membrane dynamics

class Carriers : public WallReaction {

 public:
  virtual void operator()(Wall *w, double *dw1, double *dw2) {

// PIN internalization rates
    double khij=0.;
    double khji=0.;

    double U1=0; double U2=0; double D=0;

// Calculate steady-state bound receptors levels in the apoplast

    if ((w->Apoplast(0) > 0) || (w->Apoplast(1) > 0)) {

      double ratio_a =  w->Apoplast(0) ;

      double ratio_b =  w->Apoplast(1) ;

      U1= par->Dc * par->Dr * (ratio_a + ratio_b) + ratio_a * (par->Dc *
ratio_b + par->Dr * par->Kd);
      U2= par->Dc * par->Dr * (ratio_a + ratio_b) + ratio_b * (par->Dc *
ratio_a + par->Dr * par->Kd);


      D=2 * (par->Dr * par->Kd * (par->Kd + 0.5 * ratio_a + 0.5 *
ratio_b) + par->Dc * par->Dr * (ratio_a + ratio_b + 2 * par->Kd) + par-
>Dc * (ratio_a * ratio_b + 0.5 * ratio_a * par->kR + 0.5 * ratio_b * par-
>Kd));


// PIN internalization rates
       khij = 1 + 2 * par->RT * (U1 / D);

     khji = 1 + 2 * par->RT * (U2 / D);
```

```
    }
    else {
      khij = 1;

      khji = 1;

    }



   if ((w->C1()->Boundary() != Cell::DEAD) && (w->C2()->Boundary() !=
Cell::DEAD)) {


// PIN at the plasma membrane (due to recycling)

    double dPin1=0.; double dPin2=0.;

    dPin1 = par->k_exo * w->C1()->Chemical(2) - w->Transporters1(0) *
(par->k_endo + (par->mi / khij));

    dPin2 = par->k_exo * w->C2()->Chemical(2) - w->Transporters2(0) *
(par->k_endo + (par->mi / khji));

// AUX/LAX at the plasma membrane (due to recycling)

    double dAux_Lax_1=0.; double dAux_Lax_2=0.;

    dAux_Lax_1 = par->a_exo * w->C1()->Chemical(3) - par->a_endo * w-
>Transporters1(1);

    dAux_Lax_2 = par->a_exo * w->C2()->Chemical(3) - par->a_endo * w-
>Transporters2(1);

    dw1[0] = dPin1;
    dw2[0] = dPin2;
    dw1[1] = dAux_Lax_1;
    dw2[1] = dAux_Lax_2;
   }

// Ablated Cells
      if (w->C1()->Boundary() == Cell::DEAD){

            dw1[0] -= w->Transporters1(0); // PINS
            dw1[1] -= w->Transporters1(1); // AUX/LAX

      }

      if (w->C2()->Boundary() == Cell::DEAD){

          dw2[0] -=w->Transporters2(0); // PINS
```

```
            dw2[1] -= w->Transporters2(1); // AUX/LAX

      }

}
};


 // custom functions that gives intracellular PIN and AUX/LAX levels
inline double complex_PIN(Cell &here, Cell &nb, Wall &w) { return
here.Chemical(2) ;}

inline double complex_AUX(Cell &here, Cell &nb, Wall &w) { return
here.Chemical(3) ;}

// custom functions that calculate PIN internalization rates khij and
khji
inline double inhibit_khij(Cell &here, Cell &nb, Wall &w) {

    double U1=0; double U2=0; double D=0; double khij;

// Calculate steady-state bound receptors levels in the apoplast

    if ((w.Apoplast(0) > 0) || (w.Apoplast(1) > 0)) {

      double ratio_a =  w.Apoplast(0) ;

      double ratio_b =  w.Apoplast(1) ;

      U= par->Dc * par->Dr * (ratio_a + ratio_b) + ratio_a * (par->Dc *
ratio_b + par->Dr * par->Kd);

      D=2 * (par->Dr * par->Kd * (par->Kd + 0.5 * ratio_a + 0.5 *
ratio_b) + par->Dc * par->Dr * (ratio_a + ratio_b + 2 * par->Kd) + par-
>Dc * (ratio_a * ratio_b + 0.5 * ratio_a * par->kR + 0.5 * ratio_b * par-
>Kd));

      // PIN internalization rates
       khij = 1 + 2 * par.inhibition_effect *  (U / D);
    }
    else {
      khij = 1;
    }

  return w.Transporters1(0) * (par->k_endo + (par->mi / khij)) ;
}
inline double inhibit_khji(Cell &here, Cell &nb, Wall &w) {

   double U1=0; double U2=0; double D=0; double khji;

// Calculate steady-state bound receptors levels in the apoplast

    if ((w.Apoplast(0) > 0) || (w.Apoplast(1) > 0)) {
```

```
      double ratio_a =  w.Apoplast(0) ;

      double ratio_b =  w.Apoplast(1) ;

      U= par->Dc * par->Dr * (ratio_a + ratio_b) + ratio_b * (par->Dc *
ratio_a + par->Dr * par->Kd);

      D=2 * (par->Dr * par->Kd * (par->Kd + 0.5 * ratio_a + 0.5 *
ratio_b) + par->Dc * par->Dr * (ratio_a + ratio_b + 2 * par->Kd) + par-
>Dc * (ratio_a * ratio_b + 0.5 * ratio_a * par->kR + 0.5 * ratio_b * par-
>Kd));

      // PIN internalization rates
       khji = 1 + 2 * par.inhibition_effect *  (U / D);

      }
    else {
      khji = 1;
    }

  return w.Transporters1(0) * (par->k_endo + (par->mi / khji)) ;

}



// Interface class for intracellular dynamics
class AuxinAndDifferentiation : public CellReaction {


 public:
  virtual void operator()(Cell *c, double *dchem) {


    double dPidt = 0.;
    double dAUX = 0.;


    double sum_Aux = c->SumTransporters( 2 ); // sum total levels of
AUX/LAX (intracellular and plasma membrane)

// Note: ReduceCellAndWalls is template c++ function implemented in Cell
class within Virtual Leaf framework. Its source code is upon request.

/* template<class P, class Op> P ReduceCellAndWalls(Op f, Op f1) {
      P sum = 0;
      for (list<Wall *>::const_iterator w=walls.begin();
         w!=walls.end();
         w++) {
      sum += (*w)->c1 == this ?
        f( *((*w)->c1), *((*w)->c2), **w ) :
        f1( *((*w)->c2), *((*w)->c1), **w );
```

```
      }
      return sum;
    }
*/

// PIN recycling
    dPidt = -par->k_exo * c->ReduceCellAndWalls<double>( complex_PIN ) +
c->ReduceCellAndWalls<double>( inhibit_khij, inhibit_khji);




// auxin-dependent PIN expression
    dPidt +=  par->alpha_pin * c->Chemical(0) / (par->km + c-
>Chemical(0)) - c->Chemical(2) * par->delta_pin;



// AUX/LAX recycling
    dAUX = -par->a_exo * c->ReduceCellAndWalls<double>( complex_AUX ) +
par->a_endo * sum_Aux;

// auxin-dependent AUX/LAX expression
    dAUX += par->alpha_aux * c->Chemical(0) / (par->km + c->Chemical(0))
- c->Chemical(3) * par->delta_aux;

// Ablated cells
    if (c->Boundary() == Cell::DEAD){

            dchem[2] -= c->Chemical(2);
            dchem[3] -= c->Chemical(3);

      }
      if (c->Boundary() != Cell::DEAD) {
      dchem[2] = dPidt;
      dchem[3] = dAUX;

    }
  }



};



// Example of interface classes for tissue growth rules

class CellHouseKeeping {
public:
  void operator() (Cell &c) const {
```

```
// Check if cell should divide - it reaches cartain threshold
      c.CheckForDivision(); // see below

// Example of growth rules in Virtual Leaf (VL) framework expand if auxin
concentration is low, not provascular cells
    if (c.Chemical(0) < par->threshold_growth ) {
            c.EnlargeTargetArea(par->cell_expansion_rate);
// EnlargeTagetArea is Cell object function implemented in Virtual Leaf
framework. The code is upon request.
/* This function is based on modification of cellular pott models (CPM)
applied to model plant morphogenesis:
 For more informations on  see:

 "Simulation of Biological Cell Sorting Using a Two-Dimensional Extended
Potts Model," Francois Graner and James A. Glazier, Physical Review
Letters 69, 2013-2016 (1992).

 Roeland M.H. Merks, Alfons G. Hoekstra, Jaap A. Kaandorp, Peter M.A.
Sloot, and Paulien Hogeweg, 2006.
Problem-Solving Environments for Biological Morphogenesis. Computation in
Science and Engineering, 8(1), 61-72.

Book chapter
Ariel Balter, Roeland M.H. Merks, Nikodem J. Poplawski, Maciej Swat and
James A. Glazier. 2008.
The Glazier–Graner–Hogeweg Model: Extensions, Future Directions, and
Opportunities for Further Study.
In: Katarzyna A. Rejniak, Alexander Anderson and Mark Chaplain (eds).
Single Cell Based Models in Biology and Medicine. Birkhaüser-Verlag,
Basel, Boston and Berlin. Series "Mathematics and Biosciences in
Interaction." Chapter (ii).3. pp. 137-150.


 */
    }

}
};

// Example of Color coding rules for Cell class
void Cell::SetColor(QColor &color1,QColor &color2) {

// Green: Auxin  in the cell
double tr = Chemical(0);
double h1 = 0; double s1 = 0; double v1 = 0;
double h2 = 0; double s2 = 0; double v2 = 0;

h1=120;
s1=255;
v1= 255*(tr/(1+tr));

    color1.setHsv( h1,s1,v1);
      color2.setHsv( h1,s1,v1);
```

```
}


// Check if divide
void Cell::CheckForDivision(void) {

            if (Area() >  par.cell_division_threshold ) {

                  Divide();
// Divide function are implemented in Cell class within VL framework. The
code is upon request. The algorithm is searching for the shortest
distance between two subsequent cell wall to estalish axis of cell
division.
// Area gives cell area of cell polygon
//http://mathworld.wolfram.com/PolygonArea.html


            }



}

// Example: Adjust chemicals in daughter cells

void Cell::OnDivide(ParentInfo &parent_info, Cell &daughter) {

      //cerr << "Calling Cell::OnDivide()" << endl;

      // Auxin distributes between parent and daughter according to area
      double area = Area(), daughter_area = daughter.Area();
      double tot_area = area + daughter_area;
      chem[0]*=(area/tot_area);
      daughter.chem[0]*=(daughter_area/tot_area);

            // For lack of detailed data, or a better rule, we assume
that new cells are initialy apolar
      // after division
      // So the PIN and AUX/LAX are redistributed according to the
original polarization over the walls

      // parent_info contains info about the parent
      // redistribute the PIN and AUX/LAX in the endosome according to
area

      chem[1] = parent_info.PINendosome*(area/tot_area);
      daughter.chem[1] =
parent_info.PINendosome*(daughter_area/tot_area);
      chem[2] = parent_info.PINendosome*(area/tot_area);
      daughter.chem[2] =
parent_info.PINendosome*(daughter_area/tot_area);
```

```
	for (list<Wall *>::const_iterator w=walls.begin();
	       w!=walls.end();
	       w++) {


	      // reset transporter value
	      (*w)->setTransporter(this, 1, 0.);
	      (*w)->setTransporter(this, 0, 0.);


	}

	for (list<Wall *>::const_iterator w=daughter.walls.begin();
	       w!=daughter.walls.end();
	       w++) {
	      // reset transporter value
	      (*w)->setTransporter(&daughter, 1, 0.);
	      (*w)->setTransporter(&daughter, 0, 0.);



	}

}
```